USDOT Region V Regional University Transportation Center Final Report

NEXTRANS Project No 008IY01

Pavement Damage Due to Different Tire and Loading Configurations on Secondary Roads

By

Imad L. Al-Qadi, Principal Investigator
Founder Professor of Engineering
University of Illinois, Urbana-Champaign
alqadi@uiuc.edu

and

Hao Wang
Graduate Research Assistant
Civil and Environmental Engineering
University of Illinois, Urbana-Champaign
Haowang4@illinois.edu

Report Submission Date: October 15, 2009

DISCLAIMER

Funding for this research was provided by the NEXTRANS Center, Purdue University under Grant No. DTRT07-G-005 of the U.S. Department of Transportation, Research and Innovative Technology Administration (RITA), University Transportation Centers Program. The contents of this report reflect the views of the authors, who are responsible for the facts and the accuracy of the information presented herein. This document is disseminated under the sponsorship of the Department of Transportation, University Transportation Centers Program, in the interest of information exchange. The U.S. Government assumes no liability for the contents or use thereof.

USDOT Region V Regional University Transportation Center Final Report

TECHNICAL SUMMARY

NEXTRANS Project No 008IY01 Final Report, October 2009

Pavement Damage Due to Different Tire and Loading Configurations on Secondary Roads

Introduction

Due to the large percentage of goods moved by commercial trucks and its ever-growing freight industry, the U.S. needs innovative technologies to improve the efficiency of trucking operations and ensure continuous growth of the economy. One example of such a technology is the introduction of wide-base single tires to replace conventional dual tire systems. After more than two decades of research powered mainly by the tire industry, a new generation of wide-base tire was recently introduced. Compared to the first generation of wide-base tires, these new tires offer safety and cost-savings characteristics. Despite the significant advancements achieved through previous research projects on the impcat of wide-base tires on pavements, past investigations have not evaluated the damage wide-base tires cause to low-volume secondary roads. This pavement class is widely encountered in many trucking applications, although for short distances, but the impact of the new generation of wide-base tires on these pavement structures is unclear. In addition, the static uniform loading assumption used in conventional flexible pavement design methods is inconsistent with realistic tire loading conditions and may result in erroneous pavement response and damage predictions. To address these shortcomings, this research project uses a developed three-dimensional (3-D) finite element model to predict pavement responses to loading applied by various tire configurations on secondary road pavements. This model incorporates the measured 3-D tire-pavement contact stresses, hot-mix asphalt (HMA) linear viscoelasticity, continuous moving load, and utilizes implicit dynamic analysis. The impact of wide-base tires on secondary road pavement damage was analyzed using available damage models, and the results were compared to the damage from conventional dual-tire assemblies.

Findings

Due to the different contact stress distributions at tire-pavement interface, the impact of the new generation of wide-base tire (455/55R22.5) on secondary road pavements varies when compared to the impact of the conventional dual-tire assembly. Results showed that the 455 wide-base tire causes 1.9-2.5 times more fatigue damage, 1.31-2.35 times more subgrade rutting, and 1.35-1.77 times more HMA rutting (densification) compared to the conventional dual-tire assembly when carrying the same load.

On the other hand, the 455 wide-base tire caused 19%-78% less HMA rutting (shear) and had 4%-31% less potential for base shear failure than the conventional dual-tire assembly. These damage ratios vary with different base thicknesses, temperatures, and possibly loading. The findings indicate that wide-base tires' impact on pavement damage on secondary roads depends on the roads' predominant failure mechanisms. Therefore, a combined damage ratio was used to consider the overall effect of different failure mechanisms on pavement serviceability and to conduct a simplified pavement cost analysis. In general, the results show that using the 455 wide-base tire results in 1.12-1.38 times more damage compared to the dual-tire assembly and thus greater costs for designing and maintaining secondary road pavements. This cost ratio provides state pavement agencies a basis for implementing appropriate load regulations and road pricing for trucking operations that use wide-base tires on secondary roads. It should be noted that an earlier study concluded the wide-base tire causes less or similar damage to interstate highway pavements when compared with the dual-tire assembly. The report includes simple design examples that describe how to consider the effects of the wide-base tire in pavement design and rehabilitation practice by using the damage ratio obtained from this study.

Recommendations

This study resulted in the following recommendations:

1) Because the traditional static uniform circular loading assumption cannot differentiate between different contact areas and contact stress distributions at the tire-pavement interface, it is essential to use accurate tire-pavement interaction to predict the pavement damage caused by various tire configurations.

2) The mechanistic-empirical method is recommended to quantify the pavement damage associated with wide-base tires. The failure mode for each pavement layer needs to relate to the critical response calculated at a specific position under loading.

3) A database should be created to consider the effects of the wide-base tire on pavement damage in pavement design and rehabilitation practice by using the damage ratio concept. The database should consider various pavement structures and axle configurations.

Contacts

For more information:

Imad L. Al-Qadi
Principal Investigator
Civil and Environmental Engineering
University of Illinois, Urbana-Champaign
alqadi@uiuc.edu

NEXTRANS Center
Purdue University - Discovery Park
2700 Kent B-100
West Lafayette, IN 47906
nextrans@purdue.edu
(765) 496-9729
(765) 807-3123 Fax

www.purdue.edu/dp/nextrans

USDOT Region V Regional University Transportation Center Final Report

NEXTRANS Project No 008IY01

Pavement Damage Due to Different Tire and Loading Configurations on Secondary Roads

By

Imad L. Al-Qadi, Principal Investigator
Founder Professor of Engineering
University of Illinois, Urbana-Champaign
alqadi@uiuc.edu

and

Hao Wang
Graduate Research Assistant
Civil and Environmental Engineering
University of Illinois, Urbana-Champaign
Haowang4@illinois.edu

Report Submission Date: October 15, 2009

ACKNOWLEDGMENTS

The authors acknowledge the assistance and feedback from the members of the study advisory committee. The cost sharing provided by the Illinois Center for Transportation, NCSA, and Michelin Research and Development is greatly appreciated.

TABLE OF CONTENTS

Page

LIST OF FIGURES iv

CHAPTER 1. INTRODUCTION 6

1.1 Background and motivation 6

1.2 Study objectives and scope 8

1.3 Organization of the report 9

CHAPTER 2. FINITE ELEMENT MODELING OF PAVEMENT 10

2.1 Tire-pavement interaction 10

2.2 Pavement structure 16

2.3 Material characterization 16

2.4 Development of a 3-D FE model 20

2.5 FE model validation 26

CHAPTER 3. PAVEMENT RESPONSES ANALYSIS 29

3.1 Effect of tire configuration on pavement responses 29

3.2 Effect of temperature on pavement responses 33

3.3 Effect of base layer thickness on pavement responses 35

CHAPTER 4. PAVEMENT DAMAGE ANALYSIS 37

4.1 Pavement damage models 37

4.2 Damage ratio between various tire configurations 43

4.3 Combined damage ratio 47

4.4 Use of damage ratio in road pricing 50
4.5 Use of damage ratio in pavement design and rehabilitation.....51

CHAPTER 5. CONCLUSIONS 54
5.1 Summary and conclusions 54
5.2 Recommendations.....55

REFERENCES 57

LIST OF FIGURES

Figure Page

Figure 1.1. (a) Comparison between the First and New Generations of Wide-base Tires, and (b) Comparison between a One Tire in Dual-tire Assembly and a New-generation Wide-base Tire. 7

Figure 2.1. Tire Imprint Area for (a) One Tire of a Dual-tire Assembly and (b) New Generation of Wide-base Tire (after Al-Qadi et al. 2005). 11

Figure 2.2. Normalized Contact Stress Distributions along Tire Contact Length for (a) Vertical Contact Stresses, (b) Transverse Contact Stresses, and (c) Longitudinal Contact Stresses (Tire Moving from Left to Right). 14

Figure 2.3. Illustration of Cross-section of 3-D FE Model. 21

Figure 2.4. Schematic Illustration of Tire Moving along Pavement Surface. 22

Figure 2.5. Changing Amplitude of Vertical Contact Stresses with Time Steps for (a) Entrance Part of a Tire Rib and (b) Exit Part of a Tire Rib. 23

Figure 2.6. Schematic Illustration of Contact Stresses under Each Rib. 24

Figure 2.7. Tensile Strain Pulses under Moving Vehicle Loading. 26

Figure 3.1. Tensile Strains at the bottom of HMA at 47°C along (a) Longitudinal Direction, and (b) Transverse Direction. 30

Figure 3.2. Maximum Shear (a) Strains and (b) Stresses within HMA Layer under Two Tire Configurations at 47°C. 31

Figure 3.3. (a) Deviator Stress and (b) Bulk Stress in the Middle of Base Layer under Two Tire Configurations at 47°C. 32

Figure 3.4. (a) Compressive Strain and (b) Deviator Stress on top of Subgrade under Two Tire Configurations at 47°C. 33

Figure 3.5. Longitudinal Tensile Strain Distributions with Depth under Two Tire Configurations for Section D at (a) 25°C and (b) 47°C. 34

Figure 3.6. Vertical Shear Strain Distributions with Depth under Two Tire Configurations for Section D at (a) 25°C and (b) 47°C. 35

Figure 3.7. Maximum Strains within HMA Layer for Various Base Layer Thicknesses (a) at 25^{o}C and (b) at 47^{o}C. 36

Figure 3.8. Stresses in the Middle of Base Layer for Various Base Layer Thicknesses (a) at 25^{o}C and (b) at 47^{o}C. 36

Figure 4.1. Combined Damage Ratios Between Two Tire Configurations. 50

Figure 4.2. Additional Pavement Cost Caused by the 455 Wide-base Tire. 51

CHAPTER 1. INTRODUCTION

1.1 Background and motivation

Managing the ever-increasing freight traffic is a challenge for the United States for several reasons. First of all, because trucks consume natural resources, including fuel, and contribute to gas emissions, they have a significant impact on the environment. In addition, the loading from heavy trucks accelerates pavement deterioration. Therefore, the U.S is in need of innovative technologies that can improve the efficiency of trucking operations while minimizing the damage to the environment and the road infrastructure.

One innovative technology is the use of wide-base single tires as an alternative to conventional dual-tire assemblies. Traditionally, dual-tire assemblies have provided an adequate footprint to carry heavy loads and to distribute axle load over a large area of the pavement. However, compared to conventional dual-tire assembly, wide-base tires offer the trucking industry significant economic advantages such as improved fuel efficiency, increased hauling capacity, reduced tire cost and repair, and superior ride and comfort. Wide-base tires also compare favorably to dual-tire assemblies with respect to truck operation and safety. With respect to environmental damage, the new wide-base tires provide substantial benefits in gas emission reduction, noise reduction, and less tire material to recycle at the end of service life (Al-Qadi and Elsefi, 2007).

Although wide-base tires were designed in accordance with current pavement regulations, such as “inch-width” laws, earlier studies on a previous generation of wide-base tires (385/65R22.5 and 425/60R22.5) have concluded that using wide-base single tires would significantly increase pavement damage. For example, the first generation of wide-base tires caused 1.5 to 2.0 times more rut depth and 2.0 to 4.0 times more fatigue cracking than a dual-tire assembly carrying the same load (Huhtala et al., 1989; Bonaquist, 1992). These findings led state and pavement agencies to initially discourage

the use of wide-base single tires to ensure that economic advantages to the trucking industry would not result in adverse consequences to the road infrastructure.

However, after more than two decades of research, primarily powered by the tire industry, a new generation of wide-base tires (445/50R22.5 and 455/55R22.5) was introduced in the 2000's. This new generation of wide-base tires was introduced as causing relatively less pavement damage and providing other safety and cost-saving advantages. The new generation of wide-base tires are 15 to 18% wider than the first generation and do not require high tire inflation pressure due to their special wall design. This design provides a greater tire contact area and more uniform pressure distribution at the tire-pavement interface (Figure 1.1) (Al-Qadi et al., 2005). Although the potential benefits of the new generation of wide-base tires are exciting, the pavement damage induced by these tires needs to be quantified before their true potential impact and value are known.

(a) (b)

Figure 1.1. (a) Comparison between the First and New Generations of Wide-base Tires, and (b) Comparison between a One Tire in Dual-tire Assembly and a New-generation Wide-base Tire.

Results of COST Action 334 (2001) indicated that the new generation of wide-base tires would cause approximately the same primary rutting damage as a dual-tire assembly on primary roads and 44 to 52% more combined damage (20% primary rutting, 40% secondary rutting, and 40% fatigue cracking) on secondary roads. Al-Qadi et al. (2005) concluded that the new wide-base tires caused slightly more fatigue damage and less primary rutting damage than a dual-tire assembly, based on the studies conducted at the Virginia Smart Road. Priest et al. (2005) conducted a study at the NCAT Test Track

in Auburn, Alabama and concluded that the wide-base tire (445/50R22.5) resulted in a similar pavement fatigue life as the standard dual-tire assembly (275/80R22.5). The two aforementioned studies focused on conventional flexible pavements that are primarily used in the Interstate Highway System.

In a recently completed project sponsored by the Illinois Department of Transportation (IDOT), the effect of new tire design on full-depth pavement damage was quantified through accelerated pavement testing (APT) and finite element (FE) modeling (Al-Qadi and Wang, 2009a and 2009b). Results of the experimental program indicated that the new generation of wide-base tire (455/55R22.5): 1) Causes much less fatigue damage than the first generation of wide-base tire (425/60R22.5); 2) Causes greater fatigue damage and subgrade rutting when compared to dual-tire assemblies; and 3) Could induce less near-surface cracking and HMA rutting (shear flow) potential in thick hot-mix asphalt (HMA) layers and perpetual pavements.

The predominate failure mechanisms of secondary roads are different than those of primary roads or interstate highways. Although previous research has achieved significant advancements, it has not focused on the new wide-base tires' impact on secondary road pavements. Therefore, this study aimed to quantify the pavement damage to secondary roads caused by various tire configurations. These research findings will help state departments of transportation (DOTs) predict the impact of the new wide-base tires on the road infrastructure and, therefore, invoke reasonable load regulations and fee charges for trucking operations. The implementation of these recommendations regarding the new wide-base tire will ultimately balance economic benefits (for the trucking industry) with pavement repair costs (for state DOTs and other agencies).

1.2 Study objectives and scope

The main objective of this research was to evaluate, for dual-tire assemblies and wide-base tires, the mechanism of load distribution and their impact on secondary road pavement damage. Previous research has attempted to use the linear layered elastic theory to predict pavement damage caused by various tire configurations. The layered theory assumes a uniform stress distribution within a circular contact area. However, this analytical technique cannot reflect the difference in contact stress distribution patterns

between wide-base tires and conventional dual-tire assemblies at tire-pavement interface. To overcome these limitations, a 3-D FE model was developed to simulate the realistic tire loading on secondary road pavements. The model allows for predicting pavement responses to loading applied by various tire configurations. It incorporates measured 3-D tire-pavement contact stresses, HMA linear viscoelasticity, continuous moving load, and utilizes implicit dynamic analysis.

The analyzed pavement structures were comprised of a 76-mm HMA layer and a unbound aggregate base layer with various thicknesses (203, 305, and 457mm). The critical pavement responses under various tire configurations at intermediate and high temperatures were calculated. The impact of the new generation of wide-base tire (455/55R22.5) on secondary road pavement damage was compared to the impact of conventional dual-tire assemblies for the aforementioned pavement designs.

1.3 Organization of the report

This report is divided into five chapters. Chapter 1 introduces the research background and objective. Chapter 2 describes the development of a 3-D FE model that considers realistic tire-pavement interaction and appropriate material properties. The analysis of the pavement responses to various tire configurations at intermediate and high temperatures is presented in Chapter 3. Quantification of the pavement damage ratio due to the 455 wide-base tire as compared to the conventional dual-tire assembly is discussed in Chapter 4. The investigators' conclusions and recommendations are presented in Chapter 5.

CHAPTER 2. FINITE ELEMENT MODELING OF PAVEMENT

This chapter presents the finite element (FE) modeling of secondary road pavement structures. The tire-pavement interaction is presented in section 2.1, including the determination of contact areas and stresses. Section 2.2 introduces the analyzed pavement structure, and the material characterization of the various pavement layers is presented in section 2.3. Section 2.4 describes the development of the 3-D FE pavement model and the incorporation of the measured tire-pavement contact stresses and transient moving load, as well as the utilization of the implicit dynamic analysis. Section 2.5 discusses the validation of the developed FE model.

2.1 Tire-pavement interaction

For conventional flexible pavement analysis, the layered elastic theory is commonly used; tire loading is assumed as uniform tire-pavement contact stresses (equal to tire inflation pressure) applied through a stationary circular contact area. Unfortunately, these assumptions are inconsistent with realistic loading conditions and may result in erroneous pavement response calculation and pavement damage prediction. Al-Qadi et al. (2008) summarized the drawbacks of these assumptions:

1) When a tire loading is applied to a pavement surface, three contact stress components are generated under each tire rib: vertical, transverse, and longitudinal. The vertical contact stress is non-uniformly distributed within the tire imprint, and the peak stress is much greater than tire inflation pressure.

2) The contact area under truck tire loading is in reality closer to rectangular than circular. The circular contact area does not consider the tread pattern of the tire or the localized stress distribution under each tire rib.

3) Traffic loading is not stationary loading, but a dynamic phenomenon that involves repeated application of moving wheel loads. The vehicle speed affects the loading frequency and loading time at various pavement depths. The loading amplitude keeps changing as the tire rolls over the pavement surface, and the mass inertia forces could be excited by the transient moving loading.

Hence, the effect of dynamic moving load and localized tire-pavement contact stresses on pavement responses cannot be considered in the conventional loading assumption using the 2-D elastic layered approach. The effect of using these assumptions to predict pavement responses is minimal at a depth far from the loading area, but the resulting errors could be very high in thin pavements or near the surface of thick pavements.

Tire-pavement contact area

Many researchers have used the circular or equivalent rectangular contact areas to represent vehicle loading (Huang, 1993). Figures 2.1 (a) and (b) show schematic tire imprints for one tire of a dual-tire assembly (275/80R22.5) and a wide-base 445 tire, respectively. It is clear that the tire contact area is in reality closer to a rectangular than a circular shape, especially for a wide-base tire. The tire imprint area includes five longitudinal ribs for one tire of a dual-tire assembly and nine ribs for the new generation of wide-base tire. The rectangular contact area of each rib includes grooves between adjacent ribs. Thus, the assumptions of circular or equivalent rectangular contact areas could overestimate the net contact area when the tread pattern of the tire is not considered.

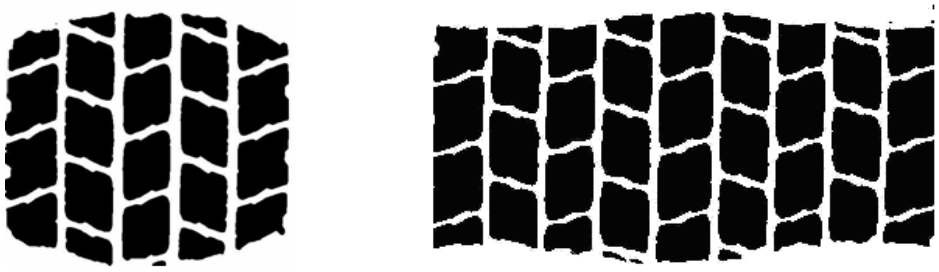

(a) (b)

Figure 2.1. Tire Imprint Area for (a) One Tire of a Dual-tire Assembly and (b) New Generation of Wide-base Tire (after Al-Qadi et al. 2005).

Three-dimensional tire contact stresses

Generally, tire-pavement contact stresses have three components: vertical, transverse, and longitudinal. An example of normalized 3-D contact stress measurements along the tire contact length under each rib of a dual 275/80R22.5 tire at free rolling condition (44kN load and 720kPa inflation pressure) on flat pavement surface is shown in Figure 2.2. The normalized peak stress magnitudes are 1207kPa, 363kPa, and 190kPa for vertical, transverse, and longitudinal contact stresses, respectively.

It is clear that the center ribs (2, 3, and 4) have longer contact lengths than the edge ribs (1 and 5). Along the longitudinal contact length of each rib, both the vertical compressive stresses and transverse tangential stresses have convex shape distributions, while the directions of longitudinal tangential stresses vary between the entrance and exit components of the tire imprint, with backward stresses in the front half of the tire and forward stresses in the rear half. The point where the longitudinal stress directions change is determined by the friction condition between the tire and pavement (Tielking and Roberts, 1987). For a free rolling condition, net longitudinal stresses for the whole contact length are not significant compared to vertical contact stresses.

The transverse distribution of contact stresses along the contact width of the tire imprint area can be observed by comparing the contact stresses under each rib. The vertical compressive stresses are usually higher underneath the center ribs (2, 3, and 4) than those under the edge ribs (1 and 5) due to the contribution of tension in the tire sidewall. Actually, the peak compressive stress under rib 3 (1207kPa) is about 1.6 times the tire inflation pressure (720kPa).

Because transverse contact stresses are mainly associated with the Poisson effect of rubber material for radial tire, transverse contact stresses have a distinct asymmetric distribution beneath each rib. The transverse contact stresses may be either tension or compression at both sides of each tire rib. Thus, the localized vertical and surface tangential stresses under each rib could affect the stress state at pavement surface and need to be considered when predicting pavement damage.

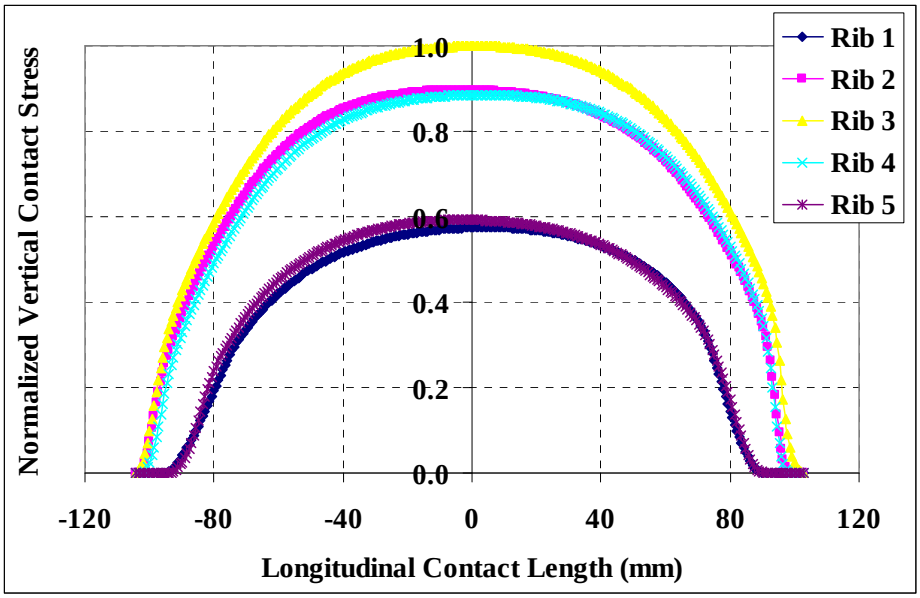
Normalized Vertical Contact Stress
1.0
0.8
0.6
0.4
0.2
0.0
-120
-80
-40
0
40
80
120
Longitudinal Contact Length (mm)
Rib 1
Rib 2
Rib 3
Rib 4
Rib 5

(a)

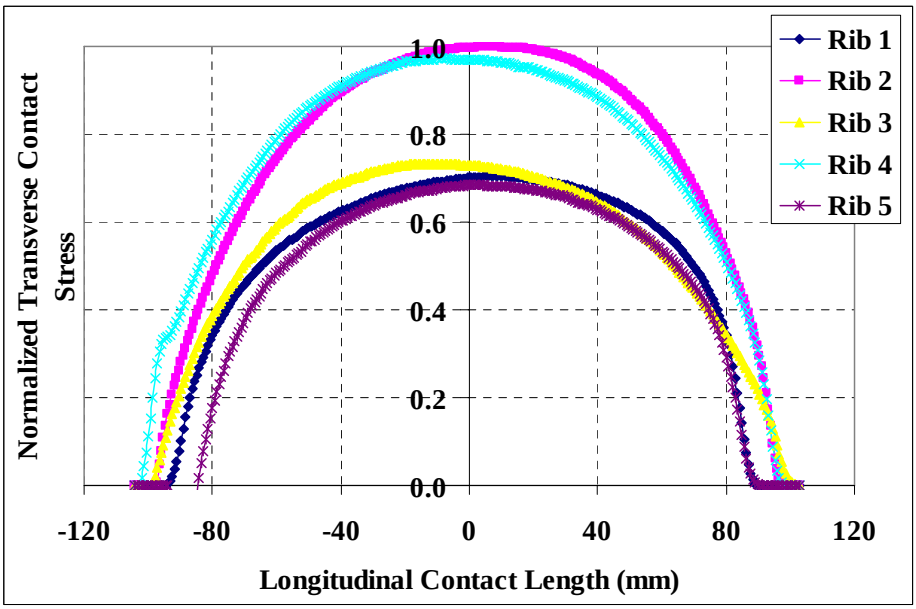
Normalized Transverse Contact Stress
1.0
0.8
0.6
0.4
0.2
0.0
-120
-80
-40
0
40
80
120
Longitudinal Contact Length (mm)
Rib 1
Rib 2
Rib 3
Rib 4
Rib 5

(b)

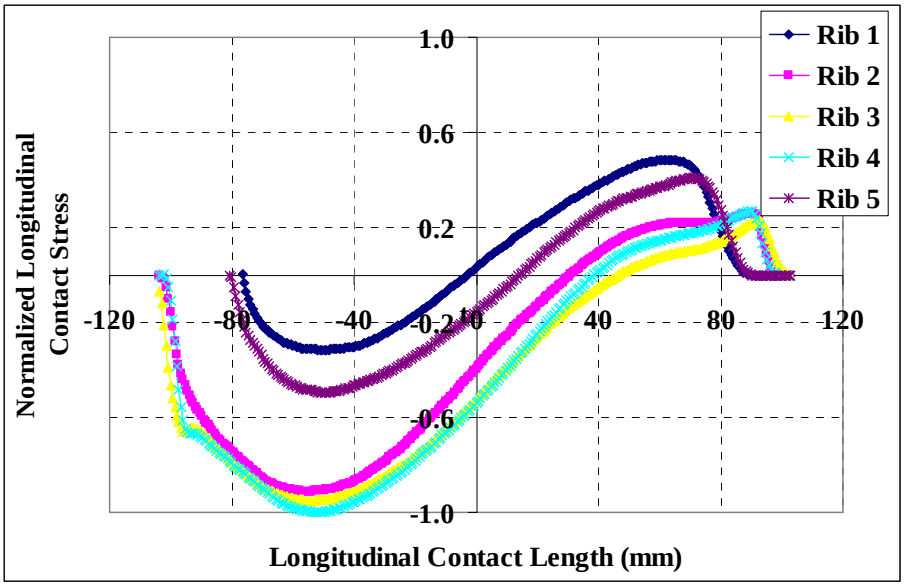

(c)

Figure 2.2. Normalized Contact Stress Distributions along Tire Contact Length for (a) Vertical Contact Stresses, (b) Transverse Contact Stresses, and (c) Longitudinal Contact Stresses (Tire Moving from Left to Right).

Contact areas and stresses of two tire configurations

Because wide-base tires and conventional dual-tire assemblies use different tire structure designs, they could have different contact areas and contact stress distributions at the tire-pavement interface. Table 1 compares the measured tire imprint areas between a dual-tire assembly and the new generation of wide-base tire (455/55R22.5) at three loading levels. This comparison shows that the 455 wide-base tire has similar net contact area with the dual-tire assembly but has longer rib contact length and less contact width. The average contact stresses are similar between the two tire configurations.

Table 1 Comparison of Tire Imprint Areas between Two Tire Configurations

Load	Tire	Net Contact Area (cm^2)	Width (mm)	Length of Middle Rib (mm)	Average Stress (kPa)
35kN	Dual-tire assembly	507	320	184	700
	Wide-base tire	517	298	198	687
44kN	Dual-tire assembly	614	320	206	725
	Wide-base tire	625	298	221	712
53kN	Dual-tire assembly	686	320	224	779
	Wide-base tire	687	298	242	778

Tables 2 compares the peak vertical and transverse contact stresses at each rib of a dual-tire assembly and the new generation of 455 wide-base tire (35kN and 720kPa). It is clear that, compared to the dual-tire assembly, the 455 wide-base tire has less vertical contact stress under the center and edge ribs. In addition, the 455 wide-base tire has relatively more uniform vertical stress distribution along the tire width. The maximum transverse contact stresses were found on both sides of each tire and vary along the tire width for both tire configurations. However, the 455 wide-base tire has lower transverse contact stresses than the dual-tire assembly, especially at the tire's edge ribs.

Table 2 Comparison of Contact Stresses between Two Tire Configurations

Peak stress under dual-tire assembly (kPa)			Peak stress under wide-base tire (kPa)		
Rib	Vertical	Transverse	Rib	Vertical	Transverse
1	594	308	1	563	139
2	1092	340	2	947	295
3	1206	256	3	882	257
4	1083	351	4	929	341
5	588	278	5	1140	244
6	588	278	6	929	313
7	1083	351	7	882	333
8	1206	256	8	947	324
9	1092	340	9	563	181
10	594	308			

2.2 Pavement structure

The secondary road pavement structures used in this study resembled those constructed for accelerated pavement testing at the Advanced Transportation Research and Engineering Laboratory (ATREL) at the University of Illinois. The analyzed pavement structures were comprised of 76-mm SM-9.5 (surface mix with maximum nominal aggregate size of 9.5mm) HMA layer and unbound aggregate base layer with various thicknesses (203, 305, and 457mm for sections A, B, and D, respectively). PG 64-22 binder was used in the SM-9.5 mix for the HMA layer. Dense-graded crushed limestone aggregates were used for the base layer. The pavement sections were constructed on subgrade with a low California Bearing Ratio (CBR) of 4%.

The test sections were instrumented to measure the pavement responses under vehicle loading. During construction, strain gauges were embedded at the bottom of the HMA layer, and linear variable deflection transformers (LVDTs) were embedded in the base layer and subgrade. Thermocouples were placed at different depths in the HMA, base, and subgrade to monitor the pavement temperature. The pavement sections were exposed to accelerated loading with different tire configurations using the Accelerated Transportation Loading ASsembly (ATLAS) housed at the University of Illinois at Urbana-Champaign. More information on construction and instrumentation of these pavement sections can be found elsewhere (Al-Qadi et al., 2007).

2.3 Material characterization

HMA viscoelasticity

To accurately predict pavement responses, the materials in each pavement layer need to be properly characterized. While elastic theory may be a reasonable approximation in the conventional design of flexible pavements, the effect of time (or frequency) and temperature dependency of HMA modulus cannot be fully considered by this approach. The time-dependent nature of HMA modulus is characterized by the fact that the stress depends not only on the current state of strain but on the full history of strain development. Generally, an integral equation model for the deviatoric and bulk

stresses is used in linear viscoelastic theory, as shown in Equations 1 and 2 (Ferry, 1980). In these equations, the relaxation modulus of HMA can be modeled as a generalized Maxwell solid in terms of a Prony series, Equations 3 and 4 (ABQAUS, 2007).

$$s = \int_{-\infty}^{t} 2G(\xi - \tau)\frac{de}{d\tau}d\tau \quad [1]$$

$$p = \int_{-\infty}^{t} K(\xi - \tau)\frac{d(tr[\varepsilon])}{d\tau}d\tau \quad [2]$$

$$G(\xi) = G_0(1 - \sum_{i=1}^{n} G_i(1 - e^{-\xi/\tau_i})) \quad [3]$$

$$K(\xi) = K_0(1 - \sum_{i=1}^{n} K_i(1 - e^{-\xi/\tau_i})) \quad [4]$$

where,

s is deviatoric stress; e is deviatoric strain;

p is volumetric stress; $tr[\varepsilon]$ is trace of volumetric strain;

G is shear modulus; K is bulk modulus; ξ is reduced relaxation time;

G_0 and K_0 are instantaneous shear and volumetric elastic modulus; and

G_i, K_i, and τ_i are Prony series parameters.

The temperature dependency of HMA modulus is characterized by the time-temperature superposition principle because HMA has been proven as a thermorheologically simple (TRS) material. The effects of time (or frequency) and temperature on HMA modulus can be combined by using the reduced time (or reduced frequency). This behavior allows for the horizontal shifting (along time or frequency axis) of the material property to form a single characteristic master curve as a function of reduced time (or frequency) at a desired reference temperature, as shown in Equations 5 and 6. The amount of horizontal shift is decided by the time-temperature shift factor. The relationship between this factor and the temperature can be approximated by the Williams-Landell-Ferry (WLF) function shown in Equation 7 (ABAQUS, 2007). When

combined with the master curve, the time-temperature shift factor allows for the prediction of the viscoelastic behavior over a wide range of conditions.

$$E(t,T) = E(\xi) \quad [5]$$

$$\xi = t / a_T \quad [6]$$

where,

t is time before shifting for a given temperature, T;

ξ is reduced time at reference temperature; and

a_T is shift factor for temperature T.

$$\log(a_T) = -\frac{C_1(T - T_0)}{C_2 + (T - T_0)} \quad [7]$$

where,

log (a_T) is log of the shift factor; T_0 is reference temperature;

T is actual temperature corresponding to the shift factor; and

C_1, C_2 are regression parameters.

In this study, the HMA relaxation modulus was inter-converted from laboratory-determined creep compliance test results based on linear viscoelastic theory (Al-Qadi et al., 2008). The shear and bulk relaxation moduli were calculated by assuming constant Poisson's ratio and then fitted into Prony series. The Prony series for relaxation modulus and the regression parameter for WLF function at reference temperature (25^{o}C) are shown in Table 3.

Table 3 HMA Viscoelastic Material Properties (25°C)

Elastic		Prony Series		WLF Function Parameters	
		G_i or K_i	τ_i		
Instantaneous Modulus (MPa)	9840	6.31E-01	2.06E-02	C1	18.1
		2.51E-01	1.73E-01		
		8.47E-02	1.29E+00		
Poisson's Ratio	0.35	2.67E-02	5.35E+00	C2	164.7
		6.66E-03	1.06E+02		

Elastic base and subgrade

The aggregate base and subgrade were assumed as linear elastic material. The resilient modulus of subgrade was estimated from its CBR value using the equation in the 2002 Mechanistic-Empirical Pavement Design Guide (MEPDG), Equation 8 (ARA, 2004). The resilient modulus of aggregate was estimated as the average measured modulus from repeated-load triaxial tests at five confining pressure levels (21, 35, 69, 104, and 138 kPa) following the AASHTO T307 procedure (Al-Qadi et al., 2007). The material properties for aggregate base and subgrade are summarized in Table 4.

$$M_R = 2555(CBR)^{0.64} \quad [8]$$

where,

M_R is resilient modulus of subgrade; and

CBR is California Bearing Ratio of subgrade.

Table 4 Material Properties for Aggregate Base and Subgrade

Material	Elastic modulus (MPa)	Poisson's ratio	Density (ton/m^3)
Aggreagate base	193	0.30	2.0
Subgrade	43	0.40	1.5

2.4 Development of a 3-D FE model

The layered elastic theory is the tool used most often to calculate flexible pavement response to truck loading due to its simplicity. In comparison to the relatively simple layered elastic theory, the Finite Element Method (FEM) can be a complex and costly analysis tool. However, the application of FE techniques allows for more accurate simulation of complex material properties and realistic tire loading. This method can consider many controlling parameters (3-D tire-pavement contact stresses, discontinuities such as cracks and shoulder joints, viscoelastic and nonlinear elastic material properties, infinite foundations, system damping, quasi-static or dynamic analysis, etc.) in the calculation of pavement responses. The FEM provides the needed versatility and flexibility to accurately predict the pavement responses under realistic tire loading.

Thus, a 3-D FE model was built using ABAQUS Version 6.7. The 3-D FE model is more appropriate, compared to the axisymmetric or 2-D plane model. It can consider the measured 3-D tire-pavement contact stress distribution under each rib and the dynamic transient loading associated with a moving vehicle. In the proposed model, the measured tire-pavement contact stresses are applied on the tire contact area, and the dynamic transient loading is captured by a continuously moving load concept and implicit dynamic analysis.

Model geometry

Since the behavior of a layered pavement system might not be approximated using truss, beam, or shell elements, 3-D continuum solid elements are often selected to simulate the problem in consideration. In this study, the eight-node, linear brick elements with reduced integration (C3D8R) were used for the finite domains, whereas infinite elements (CIN3D8) were used to reduce a large number of far-field elements without significant loss of accuracy and create a “silent” boundary for the dynamic analysis (ABAQUS, 2007). Figure 2.3 illustrates the 3-D FE model that simulates the pavement sections.

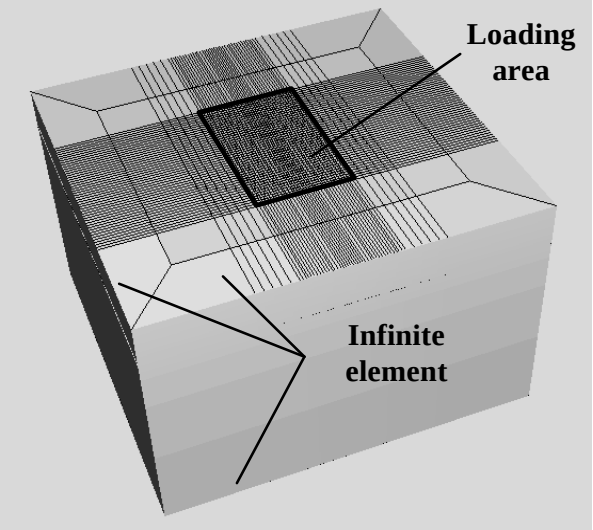

Figure 2.3. Illustration of Cross-section of 3-D FE Model.

For the FE model, a fine mesh was used around the loading area along the wheel path, and a relatively coarse mesh was used far away from the loading area. The element horizontal dimensions along the vehicle loading area were dictated by the tire rib and groove geometries. Hence, the length of elements within the loading area was selected to be 15 to 18 mm in the transverse direction and 20 mm in the longitudinal (traffic) direction. Based on the study by Yoo and Al-Qadi (2008), the element thicknesses were selected to be 9.5 mm for the HMA layers and 20 to 30 mm for the base layers.

To define the infinite boundaries at both sides, as well as the bottom of FE mesh, a sensitivity analysis was performed. After comparing the transverse and longitudinal stress/strain responses at the bottom of HMA, the horizontal location of the infinite boundary from the load center needed to be greater than 900 mm to obtain the closest solution to the full-sized reference FE model of 3 m x 3 m x 5 m (Yoo and Al-Qadi, 2008). The location of the bottom infinite boundary element was recommended to be at a depth of 1100 mm, where the maximum compressive stress in the subgrade became insignificant at 1% or less of the maximum tire-pavement contact stress.

Moving dynamic load simulation

A vehicle load applied on a pavement surface is the sum of the static load and a dynamic tire force. The dynamic tire force is the result of the vehicle's response to the longitudinal unevenness (roughness) of the road surface. To define the dynamic tire

force, intensive field measurements from vehicle axles may be needed. To characterize the transient local dynamic load without extensive field data, as in this study, the dynamic loading can be simplified by using the measured loading amplitude within the tire imprint area on a smooth pavement surface.

There are several methods that can be used to simulate the tire loading: stationary constant load; moving constant load; stationary transient load (triangle, trapezoidal, or haversine function); and moving transient load. The load applied by a tire is by nature continuously changing as a vehicle approaches and leaves a location. To simulate the movement of a tire at a certain speed, the concept of a continuously moving load was used. In this approach, the tire loading imprint area is gradually shifted over the pavement surface at each step until a single wheel pass is completed, as shown in Figure 2.4.

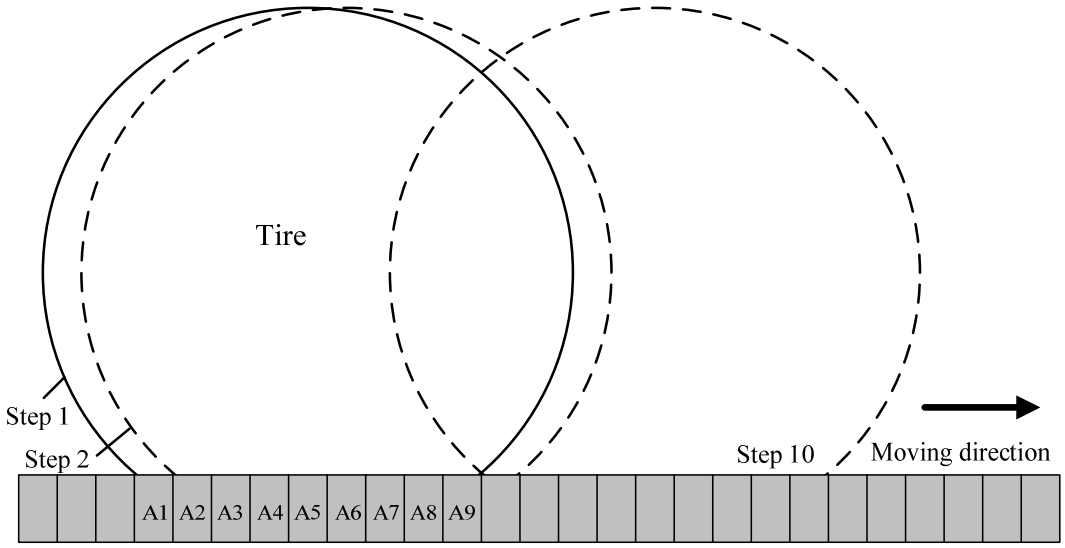

Figure 2.4. Schematic Illustration of Tire Moving along Pavement Surface.

At each step, the linear loading amplitude is applied to accurately simulate the variation of contact stress in the tire imprint area during three increments. For example, the tire imprint of rib A is composed of nine elements (A1-A9), and different loading amplitude paths are used to define the entrance and the exit components of the tire imprint, respectively. As the vehicle approaches a given element in the loading path, the element is loaded with the amplitude that simulates the increase in loading with time (Figure 2.5 (a)). Similarly, as the tire moves away from a given element, the loading amplitude that simulates the decrease in loading with time is used (Figure 2.5 (b)) (Yoo

and Al-Qadi, 2007). The step time is determined by the tire moving speed and element lengths. For each loading step, the tire imprint area is maintained constant within its influential finite-elements area.

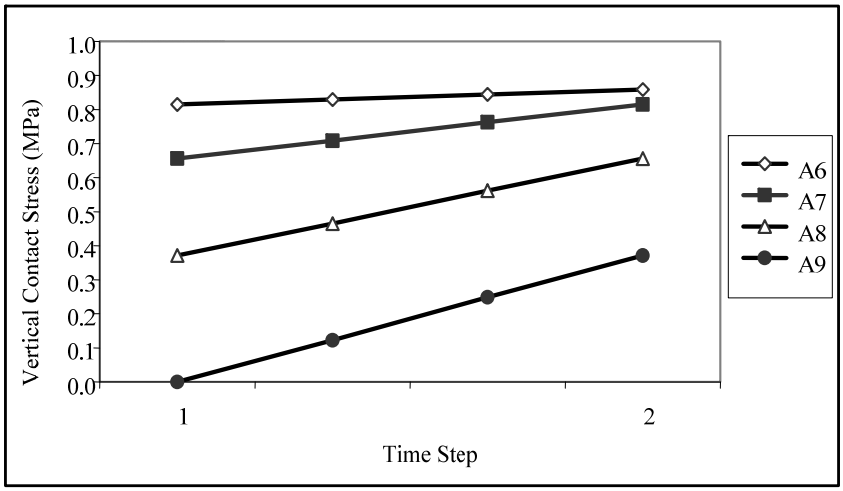

(a)

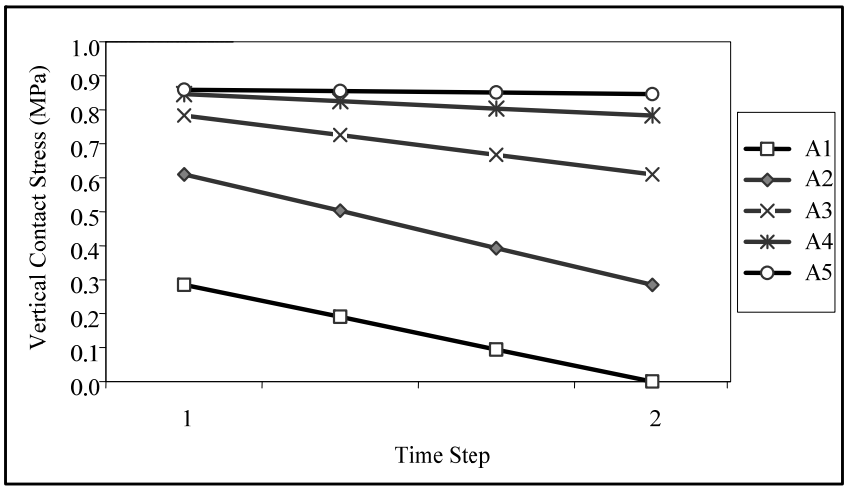

(b)

Figure 2.5. Changing Amplitude of Vertical Contact Stresses with Time Steps for (a) Entrance Component of a Tire Rib and (b) Exit Component of a Tire Rib.

Incorporation of tire-pavement contact stress

In the FE model, the measured 3-D tire-pavement contact stresses (vertical, transverse, and longitudinal) under each rib were applied on the tire imprint area, respectively (Figure 2.6). Generally, the tire imprint area of each rib includes two

elements laterally and seven to ten elements longitudinally. The exact footprint shape at a specific load level and tire pressure was considered by adjusting the number and dimension of elements within each rib. All elements along a tire rib were loaded with non-uniform vertical contact stresses corresponding to their locations within the imprint area. The loading amplitudes of vertical contact stresses continuously change at each step as the tire moves. The transverse and longitudinal contact stresses were converted into the equivalent concentrated forces using element shape functions and were assumed constant at each load step. The longitudinal contact stress was applied on the middle nodes of each rib, while the transverse contact stress was applied on the side nodes of each rib.

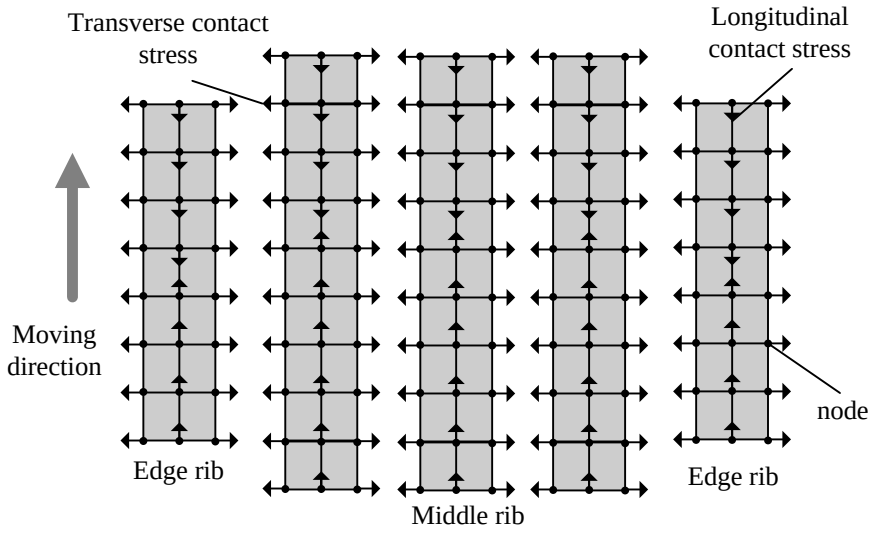

Figure 2.6. Schematic Illustration of Contact Stresses under Each Rib.

Implicit dynamic analysis

Three different approaches can be used in pavement analysis: static, quasi-static, and dynamic transient analysis. The static approach has been traditionally used in multilayer elastic analysis. The quasi-static approach is based on the concept of moving the load at subsequent positions along the pavement for each new time step, and assuming the load is static at each position. No inertia or damping effects are considered in the quasi-static analysis. In the dynamic transient analysis, two important factors need to be considered including the inertia associated with the moving load and the dependency of the material properties on the loading frequency.

The dynamic transient loading on pavement caused by a moving load is classified as a structure dynamic problem instead of a wave propagation problem, due to the fact that the vehicle speed is much less than the stress wave propagation speed in the flexible pavement structure (OECD, 1992). The dynamic equilibrium equation (see Equation 9) can be solved by a direct integration method such as using implicit or explicit modes in ABAQUS. Using an implicit method is usually more effective for a structure dynamics problem such as this one (Bathe, 1996).

$$[M]\{\ddot{U}\}+[C]\{\dot{U}\}+[K]\{U\}=\{P\} \quad [9]$$

where,

$[M]$ is mass matrix; $[C]$ is damping matrix;

$[K]$ is stiffness matrix; $\{P\}$ is external force vector;

$\{\ddot{U}\}$ is acceleration vector; $\{\dot{U}\}$ is velocity vector; and

$\{U\}$ is displacement vector.

The energy dissipation rules among an arbitrary damping factor, a friction factor, or a viscoelastic material behavior can be defined in the dynamic analysis. In the case of using viscoelastic material behavior for an HMA layer, it is not necessary to introduce additional structural or mass damping rules for that layer. The damping ratio of 5% and the Rayleigh damping scheme were used for the subgrade (Chopra, 2001).

Interface model

Contact conditions at layer interfaces are also critical parameters that significantly affect pavement responses to vehicular loading. The Coulomb friction model was used at the HMA-base and base-subgrade interfaces. This model assumes that the resistance to movement is proportional to the normal stress at an interface. In this case, the interface may resist movement up to a certain level of shear strength and then interfaces start to slide relative to one another. If the relative motion occurs, the frictional stress will keep constant.

The coefficient of friction (μ) is defined as a positive number representing the slope of the relationship between the allowed maximum shear stress (shear strength) and the normal stress, Equation 10.

$$\mu = \tau_{max} / \sigma \qquad [10]$$

where,

τ_{max} is allowed maximum shear stress before interface slide; and

σ is normal stress at the interface.

2.5 FE model validation

An example of calculated tensile strain pulses at the bottom of HMA under a moving load was plotted in Figure 2.7. As expected, the longitudinal strain was composed of a compressive component followed by a tensile component and then another compressive component, while the transverse strain is purely tensile. In addition, the transverse tensile strain shows slow recovery when the tire is leaving. Thus a relatively longer tensile time period is spent during the transverse strain compared to the longitudinal strain.

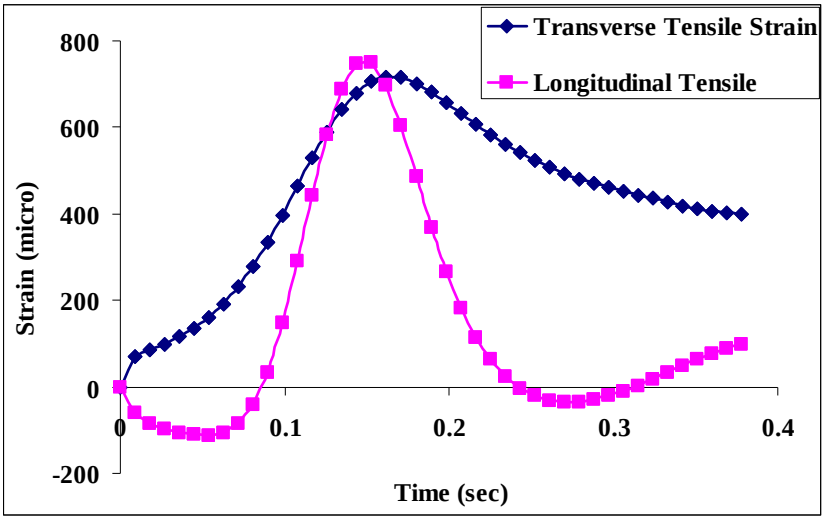

Figure 2.7. Tensile Strain Pulses under Moving Vehicle Loading.

The accuracy of FE analysis is affected by mesh dimensions, element definitions, element aspect ratios, complexity of the material models, and the evaluation location. The

level of accuracy of the developed FE model was first checked by comparing the FE solutions with the closed-form solution through a layered elastic theory based on general assumptions (e.g., static loading, fully bonded interface conditions, uniform circular contact stress, and linear elastic material behavior) (Al-Qadi and Wang, 2009).

After that, the calculated pavement responses from the three sections were compared with the field measurements at 47 ^{o}C (35.5 kN, 690 kPa and 8 km/h), respectively for the tensile strain at the bottom of the HMA layer, the compressive strain on top of the subgrade, and the vertical pressure at the bottom of the base layer (Table 5). The predicted and measured tensile and compressive strains for section D were found to be in good agreement, while the calculated strain values were smaller than the measured values for sections A and B. The calculated pressure values were greater than the measured values for all three sections. The discrepancies between the measured and predicted values could be due to the nonlinear anisotropic stress-dependency of granular material and the viscoplasticity of HMA, which were not considered in the analysis. The effect was more pronounced in sections A and B; both have thin HMA layers and weak base support.

The purpose of this study was to compare the pavement responses under various tire configurations. Table 6 presents the predicted to measured pavement response ratios. The response ratio is the pavement response to the 455 wide-base tire compared to that caused by dual-tire assembly under the same loading condition. A good agreement of response ratios was achieved for both predicted and measured values for the three sections. Hence, using relatively simple material constitutive models (viscoelastic HMA and elastic aggregate base and subgrade) were thought to be acceptable in this study at a reasonable computation cost.

Table 5 Response Comparison between Predictted and Measured Values

Sections	A		B		D	
Pavement responses from	Field	FEM	Field	FEM	Field	FEM
Transverse tensile strain at bottom of HMA	2116	1005	1727	945	707	717
Vertical pressure at bottom of base	53	73	44	66	35	56
Compressive strain at top of subgrade	/	1156	1656	1094	727	795

Table 6 Comparison of Response Ratios between Predictted and Measured Values

Sections	A		B		D	
Pavement responses ratios for	Field	FEM	Field	FEM	Field	FEM
Transverse tensile strain at bottom of HMA	1.12	1.09	1.03	1.01	0.88	0.88
Vertical pressure at bottom of base	1.36	1.24	1.33	1.23	1.16	1.17
Compressive strain at top of subgrade	/	1.21	1.17	1.10	1.10	1.07

CHAPTER 3. PAVEMENT RESPONSES ANALYSIS

Chapter 3 analyzes the calculated pavement responses to loading applied by various tire configurations. In section 3.1, the critical pavement responses (tensile, compressive, and shear stress/strain) caused by two tire configurations (dual-tire assembly and 455 wide-base tire) are compared. The effect of temperature on pavement responses is analyzed in section 3.2. In section 3.3, the effect of base thickness on pavement responses is analyzed.

3.1 Effect of tire configuration on pavement responses

The critical responses of the three pavement sections with different base layer thicknesses under two tire configurations (455 wide-base tire and dual-tire assembly) were calculated and compared, including tensile and shear strains in the HMA layer, bulk and deviator stresses in the base layer, and compressive stress and strain on top of the subgrade.

Tensile strain in HMA layer

The tensile strains at the bottom of the HMA layer are usually considered responsible for bottom-up fatigue cracking. Figures 3.1 (a) and (b) show the calculated maximum transverse and longitudinal tensile strains at the bottom of the HMA under a dual-tire assembly and a 455 wide-base tire (35.5 kN, 690 kPa, 8 km/h, 47 °C) for three pavement sections. The presented tensile strains were located under the middle tire rib of one tire in a dual-tire assembly, where the maximum vertical contact stress exists.

It is clear that the tensile strains decrease as the base layer thickness increases for both tire configurations. The longitudinal tensile strains caused by the 455 wide-base tire

are greater than the longitudinal tensile strains caused by the dual-tire assembly regardless of base thickness, while the transverse tensile strains caused by both tire configurations are relatively similar compared to the difference in longitudinal tensile strains. Compared to the dual-tire assembly, the 455 wide-base tire causes slightly greater transverse tensile strains in the pavement section with the thinnest base layer, but causes slightly less transverse tensile strains in the pavement section with the thickest base layer. The strain differences between the two tire configurations could be due to the wheel spacing between the tires in the dual-tire assembly although the two tire configurations have similar average contact stress under the same load.

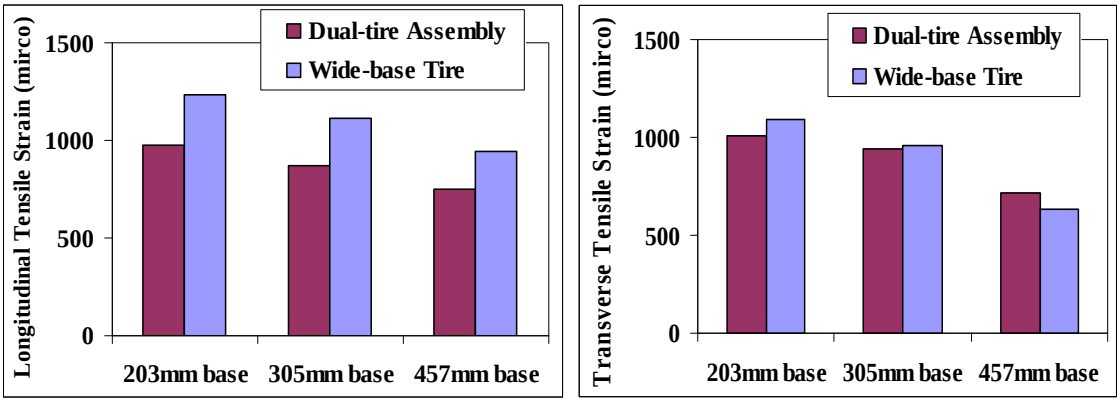

(a) (b)

Figure 3.1. Tensile Strains at the bottom of HMA at 47 °C along (a) Longitudinal Direction, and (b) Transverse Direction.

Shear stresses and strains in the HMA layer

In addition to tensile strains, the shear strains in the HMA layer are very important parameters that indicate the potential for shape distortion. Figures 3.2 (a) and (b) compare the calculated maximum vertical shear strains within the HMA layer under a dual-tire assembly and a 455 wide-base tire (35.5 kN, 690 kPa, 8 km/h, 47 °C) for the three pavement sections.

The presented vertical shear strains were located within the pavement below the tire's edge, where the maximum shear stress exists. The results show that the 455 wide-

base tire causes lower vertical shear stresses and strains than the dual-tire assembly regardless of base thickness. This could be because the 455 wide-base tire has lower surface tangential stresses at the tire edge ribs compared to dual-tire assembly, which significantly affects the pavement responses at near-surface.

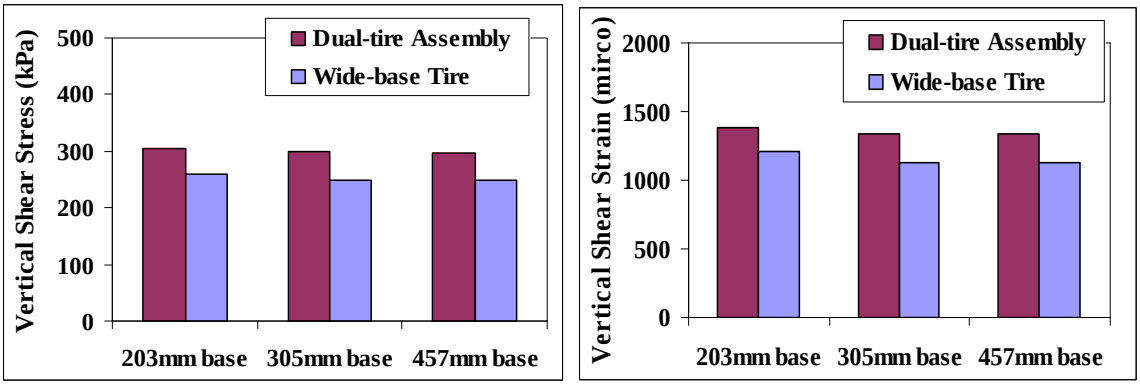

(a) (b)

Figure 3.2. Maximum Shear (a) Strains and (b) Stresses within HMA Layer under Two Tire Configurations at 47°C.

Stresses in unbound base layer

It is documented that the stress state in the middle of the unbound base layer indicates the development of deformation (Van Gurp and Van Leest, 2002). Figures 3.3 (a) and (b) show the bulk and deviator stresses in the middle of the base layer under a dual-tire assembly and a 455 wide-base tire (35.5 kN, 690 kPa, 8 km/h) at 47 °C for the three pavement sections. The deviator and bulk stresses were calculated from the principal stresses using Equations 11 and 12. The 455 wide-base tire caused greater deviator and bulk stresses in the base layer. A greater deviator stress increases the shear failure potential in the base layer, while a greater bulk stress could provide more confinement and restrict the shear failure.

$$\sigma_d = \sigma_1 - \sigma_3 \quad [11]$$

$$\theta = \sigma_1 + \sigma_2 + \sigma_3 \quad [12]$$

where,

σ_d is deviator stress;

θ is bulk stress;

σ_1 is major principal stress (compressive stress is positive);

σ_1 is intermediate principal stress; and

σ_1 is minor principal stress.

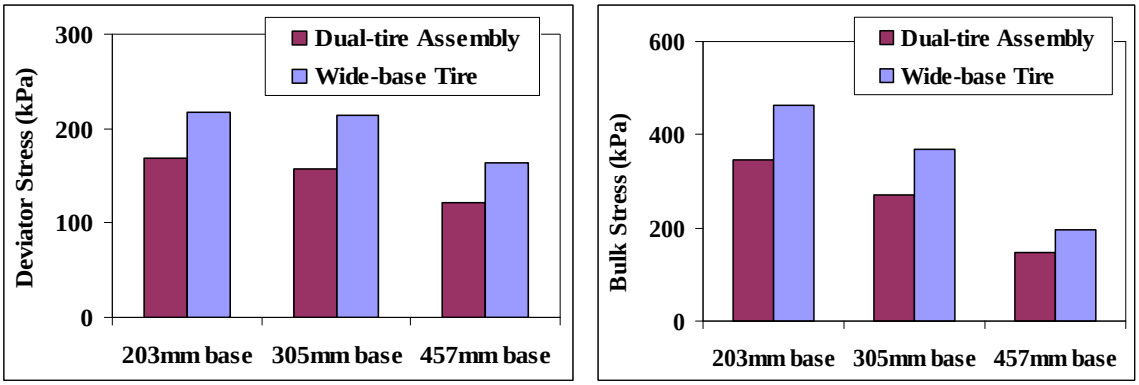

(a) (b)

Figure 3.3. (a) Deviator Stress and (b) Bulk Stress in the Middle of Base Layer under Two Tire Configurations at 47 °C.

Stresses and strains on top of subgrade

Figures 3.4 (a) and (b) compare the compressive strains and deviator stresses, respectively, on the top of subgrade under a dual-tire assembly and a 455 wide-base tire (35.5 kN, 690 kPa, 8 km/h) at 47 °C for the three pavement sections. For both tire configurations, the compressive strains and deviator stresses decrease as the base layer thickness increases. The results show that the 455 wide-base tire causes greater compressive strain and deviator stress on top of subgrade than the dual-tire assembly. As the pavement thickness increases, the differences in both strains and stresses between the two tire configurations decrease.

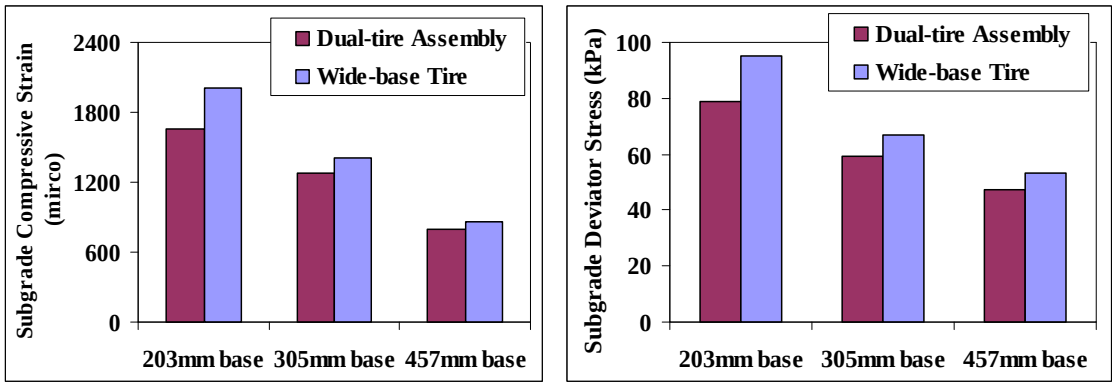

(a) (b)

Figure 3.4. (a) Compressive Strain and (b) Deviator Stress on top of Subgrade under Two Tire Configurations at 47°C.

3.2 Effect of temperature on pavement responses

The HMA stiffness is greater at low temperatures and lower at high temperatures due to its viscoelastic nature. This affects the pavement responses of the HMA layer and the underlying layers. However, the HMA layer responses are more affected by the temperature because the base layer and subgrade were modeled as elastic materials.

Figures 3.5 (a) and (b) show the longitudinal tensile strain distributions with depth for section D under two tire configurations (35.5 kN, 690 kPa, 8 km/h) at 25°C and 47 °C, respectively. The presented tensile strains are located under the middle rib of one tire in a dual-tire assembly where the maximum vertical contact stress exists. As expected, the longitudinal tensile strain distribution is compressive in the upper half of the HMA layer and becomes tensile in the lower part of the layer. The highest tensile strain was obtained at the bottom of the HMA layer at both intermediate and high temperatures. An interesting observation is that the location where the longitudinal strain changes its direction from compression to tension moves from the middle-depth of the HMA layer at 25 °C to the shallow-depth of the HMA layer at 47 °C. This indicates that a greater HMA area is exposed to the tensile stress state as temperature increases, in addition to the increase of maximum tensile strains. At both temperatures, the 455 wide-base tire causes greater longitudinal tensile strains compared to the dual-tire assembly.

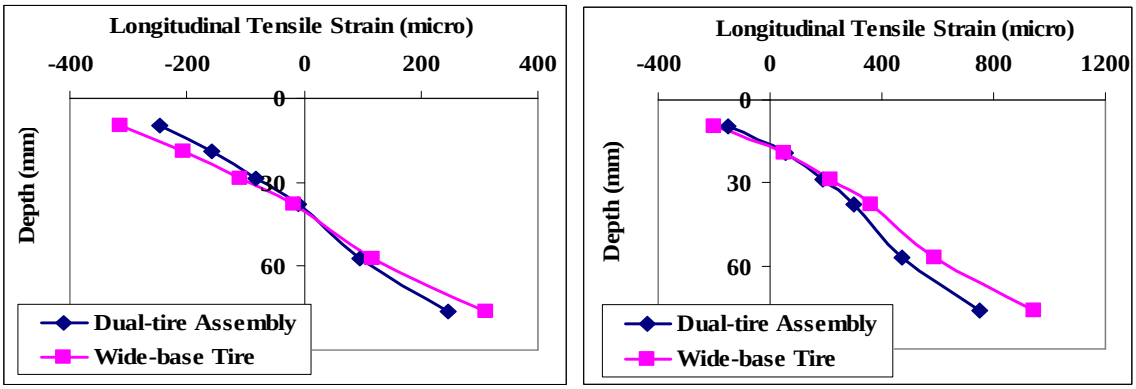

(a) (b)

Figure 3.5. Longitudinal Tensile Strain Distributions with Depth under Two Tire Configurations for Section D at (a) 25 °C and (b) 47 °C.

Figures 3.6 (a) and (b) show the vertical shear strain distributions with depth for section D under two tire configurations (35.5 kN, 690 kPa, 8 km/h) at 25 °C and 47 °C, respectively. At 25 °C, the greatest shear strain within the HMA is in the middle of the layer, while at 47 °C the greatest shear strain is in the shallow depth of the layer (around 20 mm below surface). The locations of critical shear strain are consistent with the locations where the horizontal tensile strain changes from compression to tension. At high temperature, the high magnitude of shear strain at shallow depth of the HMA layer may initiate near-surface shear cracking or may cause instable shear flow under repeated vehicle loading.

At 47 °C, the 455 wide-base tire causes much less vertical shear strain than the dual-tire assembly, while at 25 °C, the two tire configurations cause similar vertical shear strains. At intermediate temperature, the shear strain is more controlled by the load-induced bending effect, while at high temperature, the HMA becomes softer and the effect of localized tire contact stress (vertical and tangential) becomes more significant compared to the bending effect. Therefore, at 47 °C, the relatively more uniform vertical contact stress and less tangential stress at the edge of the 455 wide-base tire may result in less vertical shear strain at the tire edge compared to the dual-tire assembly.

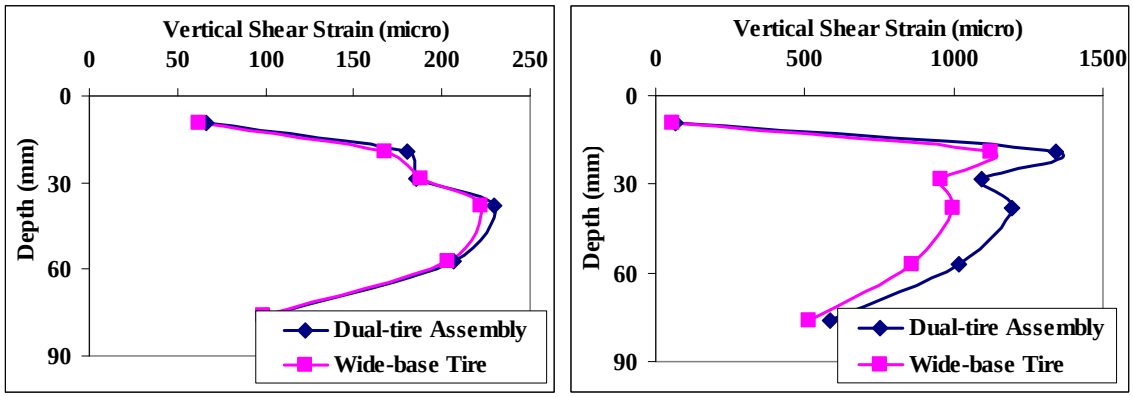

(a) (b)

Figure 3.6. Vertical Shear Strain Distributions with Depth under Two Tire Configurations for Section D at (a) 25°C and (b) 47°C.

3.3 Effect of base layer thickness on pavement responses

For low-volume roads with a thin HMA layer, the unbound aggregate base layer typically provides a significant load-carrying capacity for the pavement structure. Hence, it is important to investigate the effect of base layer thickness on pavement responses. Figures 3.7 (a) and (b) illustrate the maximum strain responses within a HMA layer for various base layer thicknesses, at 25 °C and 47 °C, respectively. The maximum tensile and compressive strains decrease as the base layer thickness increases, while the shear strain is insignificantly affected by the base layer. However, at high temperature, the maximum shear strain is much greater than the maximum tensile strain. This indicates that the shape distortion and shear deformation is predominant in the HMA layer at high temperature.

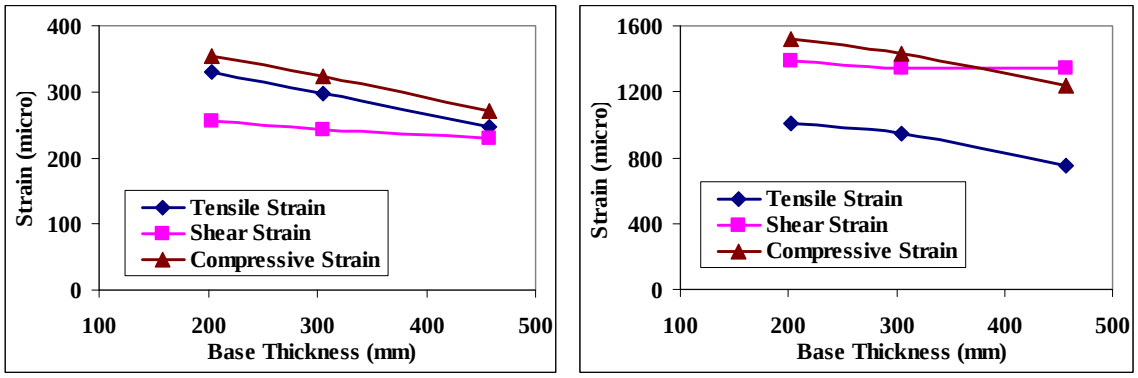

(a) (b)

Figure 3.7. Maximum Strains within HMA Layer for Various Base Layer Thicknesses (a) at 25 ^{o}C and (b) at 47 ^{o}C.

Figures 3.8 (a) and (b) show the stresses in the middle of the base layer for various base layer thicknesses, at 25 °C and 47 °C, respectively. Similarly, the bulk stress decreases as the base layer thickness increases, while the deviator stress is insignificantly affected by the base layer thickness. It should be noted that the confinement in the base layer due to the pavement self-weight was not considered; it could increase as the base layer thickness increases.

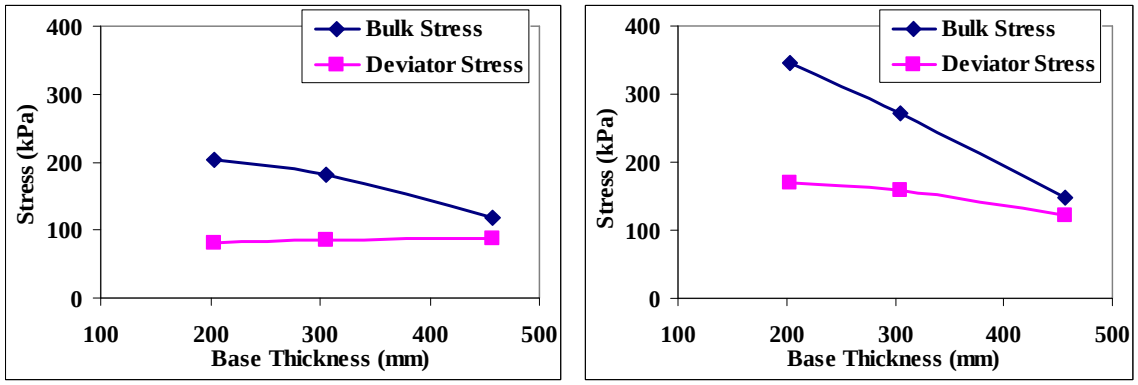

(a) (b)

Figure 3.8. Stresses in the Middle of Base Layer for Various Base Layer Thicknesses (a) at 25^{o}C and (b) at 47^{o}C.

CHAPTER 4. PAVEMENT DAMAGE ANALYSIS

This chapter compares the pavement damage caused by the wide-base tire to the damage caused by the conventional dual-tire assembly. Section 4.1 reviews the available pavement damage models for various pavement failure mechanisms, while section 4.2 presents the calculated damage ratios of the two tire configurations. Combined damage ratio is presented in section 4.3; while the costs related to the damage ratio is discussed in section 4.4. An example on the impact of using wide-base tire on costs is presented in section 4.5.

4.1 Pavement damage models

Generally, a pavement structure has three components: a HMA layer, granular or stabilized base/subbase layers, and subgrade. Each layer exhibits a unique mode of failure. The failure mode for each layer is related to that layer's critical response at a specific position under loading. In this study, pavement damage models (also called transfer functions) were used to provide the relationship between the critical pavement responses and the allowed number of load applications before failure.

For a low-volume road with a thin HMA layer, the base layer plays an important role. In addition to the traditional design criteria of limiting the horizontal strain at the bottom of the HMA layer and the vertical compressive strain at the top of the subgrade, the permanent deformation of the base layer must also be considered. The accumulation of permanent deformation in the HMA layer may be caused by densification or shear flow or a combination of both. The main failure mechanisms in each pavement layer and the available damage models for flexible low-volume roads are summarized below.

Fatigue cracking of HMA layer

The HMA surface layers usually fail in tension, whereby cracks initiate from the bottom of the HMA layer and propagate through the layer. This is known as bottom-up fatigue cracking and is one of the predominant methods of failure in thin HMA layers. Tensile strain at the bottom of the HMA layer is responsible for this type of failure mode. The tensile strain is mainly caused by the load-induced bending of the HMA layer and the inadequate structural support from the underlying layers. For thick HMA layers or perpetual pavement, the tensile strain at the bottom of the HMA layer is less critical than the shear strain near the pavement's surface (Al-Qadi et al., 2008; Wang and Al-Qadi, 2009).

The AASHTO 2002 Mechanistic-Empirical Pavement Design Guide, MEPDG, (ARA, 2004) determines the number of allowable load applications for fatigue cracking as follows:

$$N_f = 0.00432 \cdot k_1^{'} \cdot C \cdot (\frac{1}{\varepsilon_t})^{3.9492} \left(\frac{1}{E}\right)^{1.281} \quad [13]$$

$$C = 10^M \quad [14]$$

$$M = 4.84\left(\frac{V_b}{V_a + V_b} - 0.69\right) \quad [15]$$

$$k_1^{'} = \frac{1}{0.000398 + \frac{0.003602}{1 + e^{(11.02 - 3.49 \cdot h_{ac})}}} \quad [16]$$

where,

N_f is number of allowed load applications;

E is resilient modulus of HMA (psi);

ε_t is tensile strain at pavement surface;

h_{ac} is HMA thickness (in.);

V_a is air void (%) (V_a = 4% in this study); and

V_b is effective binder content by volume (%) (V_b = 5% in this study).

This method utilizes the initial pavement response and ignores the evolution of the strains with damage; however, the introduced error is considered within the empirical design framework.

Rutting of HMA layer

Two types of rutting (permanent deformation) may exist in a HMA layer simultaneously: volume reduction caused by traffic densification and aggregate particle movement with a constant volume or an increasing volume (dilation) caused by shear flow. The general form of HMA rutting models is usually derived from statistical analysis of the relationship between plastic and elastic compressive strains measured in the repeated-load uniaxial/triaxial test. The following transfer function is suggested by the AASHTO 2002 MEPDG (ARA, 2004):

$$\log(\frac{\varepsilon_p}{\varepsilon_r}) = -3.7498 + 0.4262\log(N) + 2.02755\log(T) \quad [17]$$

where,

ε_p is accumulative permanent strain (12.5 mm rutting depth was used as failure criteria in this study);

ε_r is recoverable strain;

N is allowed number of load repetitions corresponding to ε_p; and

T is pavement temperature (°C).

Monismith et al. (1994) demonstrated that the accumulation of permanent deformation in the HMA layer was very sensitive to the layer's resistance to shape distortion (i.e. shear) and relatively insensitive to volume change. Their study indicates that HMA rutting is mainly caused by shear flow rather than volumetric densification,

especially under loading of slow moving vehicles at high temperature. Deacon et al. (2002) and Monismith et al. (2006) correlated HMA rutting to shear stresses and shear strains in the HMA layer instead of compressive strain, as shown in Equation 18. This model was originally developed for Westrack mixes based on repeated simple shear test at constant height (RSST-CH).

$$\gamma = a \cdot \exp(b\tau_s)\gamma^e n^c \qquad [18]$$

where,

γ is permanent (inelastic) shear strain (12.5 mm rutting depth was used as failure criteria in this study);

γ^e is elastic shear strain;

τ_s is corresponding shear stress (in psi);

n is number of axle load applications; and

a, b, and c are experimental determined coefficients (a=1.262, b=0.05, c=0.36 were used in this study).

Permanent deformation of unbound base layer

Permanent deformation of the base layer is caused by the granular material having insufficient stability due to heavy loading or poor drainage conditions. This may result in loss of particle-to-particle interlock forces and thus the bearing capacity of base layer (shear failure). However, few design methods consider the cumulative permanent deformation or insufficient stability in granular base layer as critical.

In the South African Mechanistic Design Method (SA-MDM), the permanent deformation of the base layer is related to the ratio of the working stress to the yield strength of the material considering that high shear stress can extend into the base layer in thin-surfaced pavements for normal traffic loading (Theyse, 1996). Maree (1978) related the allowed load applications to the factor of safety by measuring the permanent deformation of granular material under dynamic triaxial loading, as shown in Equations

19 and 20. The safety factor concept was developed from the Mohr-Coulomb theory and represents the ratio of the material shear strength divided by the applied deviator stress.

$$F = \frac{\sigma_3[k(\tan^2(45+\frac{\phi}{2})-1]+2kc\tan(45+\frac{\phi}{2})}{\sigma_1-\sigma_3} \quad [19]$$

$$N = 10^{(2.605122F+3.480098)} \quad [20]$$

where,

σ_1 and σ_3 are major and minor principal stresses (compressive stress positive and tensile stress negative);

k is constant (k = 0.95 for normal moisture condition was used in this study);

c is cohesion coefficient;

ϕ is angle of internal friction (c =0, ϕ =30^o were used in this study); and

N is allowed load applications until failure.

Recent research by Theyse (2007) introduced the effects of material density and moisture content into the damage models based on a stress ratio approach similar to the factor of safety approach (see Equation 21). Although the shear stress may not exceed the shear strength under traffic loading, and shear failure will not occur under one load application, shear deformation could rapidly accumulate after a number of load repetitions leading to the evolution of damage.

$$\log(N) = 10^{1-a\frac{S^d}{SD^b}} SR^m \quad [21]$$

where,

N : Allowed load applications until failure;

S : Degree of saturation;

SD : Solidity (ratio of the volume filled with solids to the total volume);

SR : Stress Ratio at middle-depth of base layer; and

l, a, b, d, m : Regression parameters

Subgrade rutting

Subgrade rutting (secondary rutting) is a longitudinal wheel-path depression that occurs when subgrade exhibits permanent deformation caused by compressive or shear stress due to repetitive traffic loading. Usually, the vertical compressive strain at the top of the subgrade is related to subgrade rutting. The Asphalt Institute (1982) proposed a rutting damage model based on roadbed soil strain with the maximum threshold of 12.5mm rutting on subgrade, as follows:

$$N = 1.365 \times 10^{-9} (\varepsilon_v)^{-4.477} \quad [22]$$

where,

N is allowed load repetitions until failure, and

ε_v is maximum vertical compressive strain on top of subgrade.

The AASHTO 2002 MEPDG (ARA, 2004) proposed a model assuming permanent strain proportional to the resilient strain in an unbound pavement layer, as shown in Equation 23. The three parameters in the model are affected by the material properties, environmental conditions, and stress states. The model parameters can be determined by fitting a curve that relates permanent strains to loading cycles obtained from creep and recovery or repeated load triaxial tests.

$$\delta(N) = \beta_1 \left(\frac{\varepsilon_0}{\varepsilon_r} \right) e^{-\left(\frac{\rho}{N}\right)^{\beta}} \varepsilon_v h \quad [23]$$

where,

δ is permanent deformation for the layer/sub-layer;

N is allowed number of load applications until failure;

$\varepsilon_0, \beta, \rho$ are parameters depending on material properties;

ε_r is resilient strain imposed at laboratory test to obtain material properties;

ε_v is average vertical resilient strain from the primary response model;

h is thickness of the layer/sub-layer; and

β_1 is calibration factor.

Subgrade soil can also fail in shear when its shear capacity is exceeded by the applied load. Thompson (2006) used a parameter called Subgrade Stress Ratio (SSR) to estimate the rutting potential of a pavement system. The SSR is defined by Equation 24.

$$SSR = \frac{\sigma_{dev}}{q_u} \quad [24]$$

where,

SSR is Subgrade Stress Ratio;

σ_{dev} is subgrade deviator stress; and

q_u is subgrade unconfined compressive strength.

The subgrade damage potential criteria are SSR = 0.5, 0.6, 0.6-0.75, and >0.75 for low, acceptable, limited, and high ratios, respectively. Theyse (2007) concluded that the region of high shear stress does not extend down into the subgrade for normal road traffic when sufficient cover is provided to the subgrade and the relationship between the plastic and elastic strain seems to be adequate as a design criterion. In cases where extremely high aircraft loads are applied to pavement structures, the shear stress magnitude is so high that the stress ratio approach should be used.

4.2 Damage ratio between various tire configurations

It is essential that the mechanistic-empirical pavement design accurately predicts the pavement response under real vehicle loads and relates it to different damage mechanisms. The considered critical pavement responses and corresponding failure mechanisms in each pavement layer are summarized in Table 7.

Table 7 Summary of Failure Criteria in Each Pavement Layer

Layer	Material	Criterion	Location in the layer	Model of distress
Surface	HMA	Tensile strain	Bottom	Fatigue cracking
		Shear strain	Shallow depth	Rutting caused by shear flow
		Compressive strain	Bottom	Rutting caused by compression
Base	Unbound aggregate	Deviator stress	Middle	Shear failure resulting from permanent deformation
Subgrade	Soil	Compressive strain	Top	Secondary rutting

Using the calculated pavement responses from the FE model and the available damage models, Tables 8 through 12 present the calculated damage ratios caused by the 455 wide-base tire with respect to the dual-tire assembly (35.5 kN, 690 kPa, 8 km/h) at 25 ^{o}C and 47 ^{o}C, respectively, for fatigue cracking, HMA rutting caused by densification, HMA rutting caused by shear, base shear failure, and secondary rutting. The damage ratio for each specific failure mechanism was calculated using Equation 15. For fatigue cracking, shear failure, and secondary rutting, the allowable number of load applications to failure can be directly predicted from Equations 13, 20, and 22, respectively. For HMA rutting caused by densification and shear, the damage ratio is calculated as the ratio of the required load applications between two tire configurations to achieve the same plastic strain (Equations 17 and 18).

$$DR = N_{dual} / N_{w455} \quad [25]$$

where,

DR is damage ratio caused by the 455 wide-base tire with respect to the dual-tire assembly for the considered failure mechanism (fatigue cracking, HMA rutting due to densification, HMA rutting due to shear flow, base shear failure, and subgrade rutting);

N_{w455} is allowable number of load applications to failure for the 455 wide-base tire; and

N_{dual} is allowable number of load applications to failure for dual-tire assembly.

The 455 wide-base tire causes 1.91-2.50 times more fatigue damage than the conventional dual-tire assembly; the 455 wide-base tire causes greater tensile strain at the bottom of the HMA layer when carrying the same load. The 455 wide-base tire causes 1.31-2.35 times more subgrade rutting and 1.35-1.77 times more HMA rutting due to densification compared to the conventional dual-tire assembly. The 455 wide-base tire induces greater compressive strain in the HMA layer and subgrade. However, for subgrade rutting and HMA rutting due to densification, the relative damage ratios between the two tire configurations decrease as the base thickness increases.

On the other hand, the 455 wide-base tire causes much less HMA rutting due to shear flow than the conventional dual-tire assembly, especially at high temperature. The 455 wide-base tire causes less shear stress and strain, which are responsible for the accumulation of HMA rutting caused by shear flow (Equation 18), at shallow depths of the HMA layer. As for the base shear failure, the 455 wide-base tire results in less failure potential compared to the conventional dual-tire assembly. The 455 wide-base tire causes greater deviator stress, which increases the shear failure potential, but it also causes greater confinement stress, which restricts shear failure. The ratio of confinement stress with respect to deviator stress in the base layer is greater under a 455 wide-base tire than under a dual-tire assembly. This reduces the relative potential of shear failure in the unbound base layer (Equation 19).

Table 8 Damage Ratios for Fatigue Cracking between Two Tire Configurations

Temperature (^oC)	Base thickness (mm)	Critical tensile strains (micro)		Damage ratio
		Dual	Wide-base	
25	203	331	403	2.18
	305	297	364	2.23
	457	248	310	2.41
47	203	1005	1232	2.24
	305	945	1113	1.91
	457	750	946	2.50

Table 9 Damage Ratios for HMA Rutting (Densification) between Two Tire Configurations

Temperature (^{o}C)	Base thickness (mm)	Critical HMA compressive strains (micro)		Damage ratio
		Dual	Wide-base	
25	203	355	453	1.77
	305	324	412	1.76
	457	272	345	1.75
47	203	1520	1820	1.53
	305	1430	1690	1.48
	457	1240	1410	1.35

Table 10 Damage Ratios for HMA Rutting (Shear) between Two Tire Configurations

Temperature (^{o}C)	Base thickness (mm)	Critical shear strains (micro)		Critical shear stress (kPa)		Damage ratio
		Dual	Wide-base	Dual	Wide-base	
25	203	255	259	409	400	0.81
	305	243	244	397	384	0.68
	457	230	222	380	358	0.43
47	203	1389	1212	306	259	0.27
	305	1342	1124	300	249	0.22
	457	1342	1124	298	248	0.22

Table 11 Damage Ratios for Base Shear Failure between Two Tire Configurations

Temperature (^{o}C)	Base thickness (mm)	Deviator stress (kPa)		Minor principal stress (kPa)		Damage ratio
		Dual	Wide-base	Dual	Wide-base	
25	203	84	112	39	53	0.69
	305	66	111	30	40	0.92
	457	42	103	9	12	0.96
47	203	169	217	57	76	0.87
	305	158	214	35	49	0.92
	457	122	164	6	9	0.94

Table 12 Damage Ratios for Subgrade Rutting between Two Tire Configurations

Temperature (^{o}C)	Base thickness (mm)	Critical subgrade compressive strains (micro)		Damage ratio
		Dual	Wide-base	
25	203	1347	1510	1.67
	305	1134	1205	1.31
	457	770	818	1.31
47	203	1660	2010	2.35
	305	1283	1414	1.55
	457	801	856	1.35

4.3 Combined damage ratio

The distress type that allows the fewest number of load applications is expected to cause a pavement's failure. However, the calculation of the allowable number of load applications depends significantly on the local calibration factors and material parameters used in the pavement damage models. This could cause the predominant failure type to vary in different loading scenarios. Thus, a combined damage ratio was used to consider the overall effect of different failure mechanisms caused by the 455 wide-base tire with respect to the dual-tire assembly.

The combined damage ratio was calculated as a logarithmic damage distribution factor, as shown in Equations 26 and 27. The logarithmic distribution function was used to balance the effect of each failure mechanism with respect to the overall damage induced by the tire (Al-Qadi et al., 2005). This transformation is commonly used in statistics and is recommended when dealing with variables spreading over several orders of magnitude, as is the case here. In the field, even if one failure mechanism is manifested, this does not imply that the other distresses will not occur throughout the pavement service life. The failure mechanisms are progressive and contribute together to degrade the pavement serviceability. For this reason, a combined damage ratio is more appropriate and was therefore adopted in this analysis.

$$CDR = a_1 DR_{fatigue} + a_2 DR_{HMA-densification} + a_3 DR_{HMA-shear} + a_4 DR_{base} + a_5 DR_{rutting-subgrade} \quad (26)$$

$$a_i = \frac{1/\log(N_i)}{\sum_{j=1}^{n} 1/\log(N_j)} \quad (27)$$

where,

CDR = combined damage ratio caused by the 455 wide-base tire with respect to the dual-tire assembly;

$DR_{fatigue}$ = damage ratio for fatigue cracking;

$DR_{HMA-densificat\ ion}$ = damage ratio for HMA rutting due to densification;

$DR_{HMA-shear}$ = damage ratio for HMA rutting due to shear flow;

DR_{base} = damage ratio for base shear failure;

$DR_{rutting-subgrade}$ = damage ratio for subgrade rutting;

a_1, a_2, a_3, a_4, a_5 = damage distribution factors for different failure mechanisms;

N_i, N_j = allowable number of load applications for different failure mechanisms; and

n = total number of considered failure mechanisms (n=5 here).

Table 13 shows the five damage components and the corresponding distribution factors for three pavement sections at 25 ^{o}C and 47 ^{o}C. The results show that the HMA rutting due to shear flow, the subgrade rutting, and the base deformation are the predominant failure mechanisms at intermediate temperature (25 ^{o}C) depending on base thickness; while the HMA rutting due to shear flow is the most predominant failure mechanism at high temperature (47 ^{o}C). The calculated combined damage ratios caused by the 455 wide-base tire with respect to the dual-tire assembly are shown in Figure 4.1. In general, the 455 wide-base tire causes 1.12-1.38 times more damage on secondary road pavements, compared to the dual-tire assembly. The combined damage ratios decrease as the base thickness increases. At high temperature, the combined damage ratios are similar or less than those ratios at intermediate temperature.

Table 13. Damage Components and Distribution Factors

Temperature (^{o}C)	Base thickness (mm)	Fatigue Cracking	HMA Rutting (Densificaiton)	HMA Rutting (shear)	Base Deformation	Subgrade Rutting
		a_1	a_2	a_3	a_4	a_5
25	203	0.16	0.14	0.26	0.18	0.26
	305	0.16	0.15	0.25	0.20	0.24
	457	0.16	0.14	0.24	0.26	0.20
47	203	0.19	0.15	0.28	0.16	0.22
	305	0.19	0.15	0.28	0.18	0.20
	457	0.17	0.15	0.29	0.22	0.17

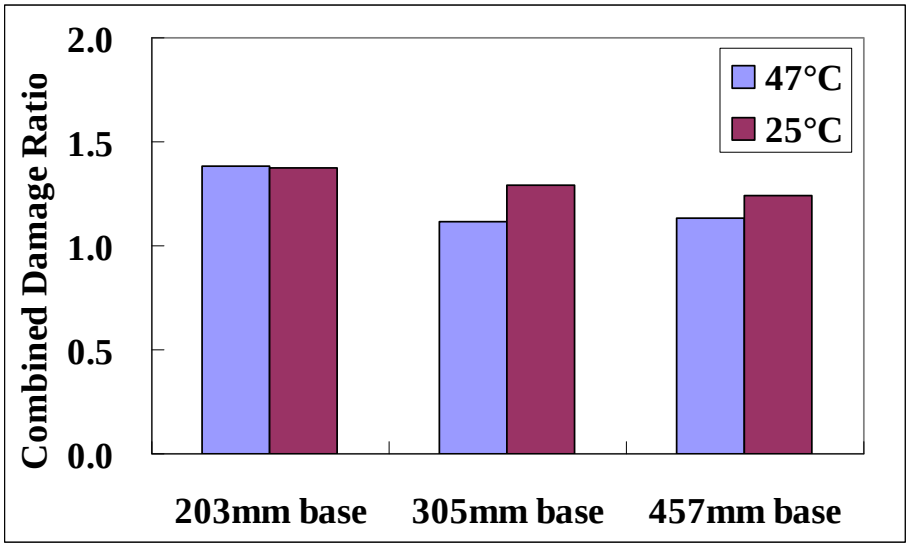

Figure 4.1. Combined Damage Ratios between Two Tire Configurations.

4.4 Use of damage ratio in road pricing

Truck loading characteristics, such as tire configurations, affect the costs highway agencies must pay to construct and maintain their pavements at an acceptable level of performance. For example, tire configurations affect pavement thickness design, overlay thickness design, and the time intervals for pavement resurfacing; all of these factors influence costs.

The calculated combined damage ratio between two tire configurations represents the equivalent number of passes of the dual-tire assembly to cause the same amount of damage as one pass of the 455 wide-base tire. Thus, the ratio can be used to compare the costs induced by two tire configurations if the load equivalency factor (LEF) and the reference cost is known. For example, the IDOT's Truck Size and Weight Report (2006) states that the pavement cost (new construction plus rehabilitation) per ESAL-mile with dual-tire assembly is \$0.508 for local roads. Using the AASHTO LEF, the pavement cost per mile per pass caused by the dual-tire assembly at 35.5 kN would be \$0.508×0.61= \$0.31. Then the pavement cost per mile per pass caused by the 455 wide-base tire at the same load would be \$0.31 multiplied by the combined damage ratio.

Figure 4.2 shows the additional pavement cost caused by the 455 wide-base tire compared to the dual-tire assembly. In general, the results show that using the 455 wide-base tire results in a greater cost ($0.04-$0.12 more per mile per pass at 35.5 kN) on secondary road pavements. The principle underlying road pricing is to charge vehicles for the damage they inflict on pavements. Thus, the estimated pavement cost provides state pavement agencies a basis for implementing appropriate load regulations and road pricing for trucking operations using wide-base tires.

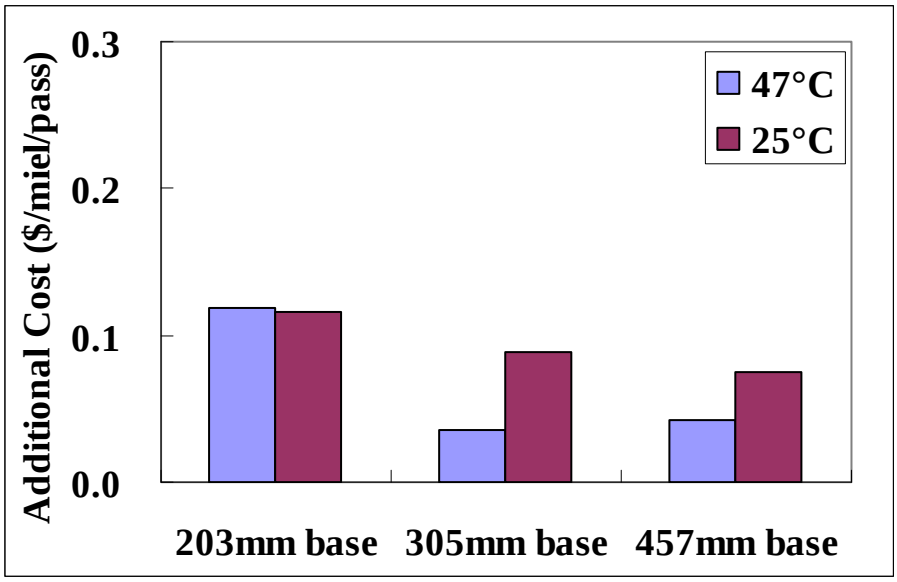

Figure 4.2. Additional Pavement Cost Caused by the 455 Wide-base Tire.

4.5 Use of damage ratio in pavement design and rehabilitation

Simple design examples are provided to describe how to consider the effects of wide-base tires in pavement design and rehabilitation practice by using the damage ratio obtained from this study. Two examples, a newly constructed pavement and an in-service pavement are discussed, respectively.

Pavement Design Example:

For a newly constructed pavement, the design steps are as follows:

Step 1: Calculate the number of axles with wide-base tires that will be applied on the pavement in the design period through traffic analysis.

Step 2: Covert the number of axles with wide-base tires to the number of axles with dual-tire assembly using the damage ratios obtained from this study.

If the pavement is designed based on a specific failure type using a mechanistic-empirical approach, the damage ratio corresponding to the specific failure mechanism can be used. For designers using the MEPDG software, the input traffic data would be the summation of the actual traffic using dual-tire assembly and the equivalent traffic that is converted from the passes of wide-base tires using the combined damage ratio.

If the pavement is designed following the AASHTO design procedure (AASHTO, 1993), the load equivalency factors for the corresponding wide-base tires can be calculated using Equation 28:

$$\text{LEF for wide-base tires at a given axle load} = \text{AASHTO LEF for the axle load} \times \text{combined damage ratio obtained from this study} \quad (28)$$

Step 3: Complete the design under current specification and procedure.

Pavement Rehabilitation Example:

For in-service pavement constructed 10 years ago with a 20-year design life, the number of design equivalent single axle loads (EASLs) was 400,000 at at the time of design. The pavement has been subjected to 200,000 ESALs since the road was opened. However, the pavement is expected to be exposed to a number of trucks with wide-base tires in the near future, and this was not expected at design.

According to the original pavement design, the remaining number of ESALs would be 200,000 and the remaining life is 10 years if the wide-base tire traffic is not considered. The new remaining life considering the traffic with wide-base tires can be calculated with the following steps:

Step 1: Calculate the LEF for wide-base tires using Equation 28.

Step 2: Calculate the remaining number of equivalent ESALs considering the traffic with wide-base tires using Equation 29:

Remaining equivalent number of ESALs = the number of axles with dual-tire assembly at a given axle load × AASHTO LEF for the axle load + the number of axles with wide-base tire at a given axle load × LEF for wide-base tires (29)

Step 3: Calculate the remaining equivalent life of the pavement considering the traffic with wide-base tires using Equation 30:

Remaining equivalent life = the original remaining life × the original remaining number of ESALs / the remaining equivalent number of ESALs (30)

For example, assume only one single axle load (35.5 kN) exists in the traffic, the allowable number of load applications with dual-tire assembly would be 200,000/0.61= 327,869. The pavement structure is assumed similar to the pavement section D (457mm base) used in this study and the design temperature is assumed 25 ^{o}C. If 10% of axles use wide-base tires and 90% of axles use conventional dual-tire assemblies, the remaining equivalent number of ESALs = 327,869 × 0.9 × 0.61 + 327,869 × 0.1 × 0.61 × 1.24 = 204,800. Thus, the remaining equivalent life = 10 × 200,000 / 204,800 = 9.8 years. This indicates that the pavement should be rehabilitated 0.2 year earlier than the original plan. Note that the remaining life is highly dependent on the proportion of the trucks using wide-base tires and the combined damage ratio.

It has to be noted that the impact of wide-base tire on interstate highway (thick pavement) is less than that on secondary roads. The combined damage ratio is expected to be less or close to unity in that case (Al-Qadi and Wang, 2009b).

CHAPTER 5. CONCLUSIONS

This chapter summarizes the research findings and recommendations.

5.1 Summary and conclusions

This study investigated the impact of the new generation of wide-base tires (455/55R22.5) on the pavement damage of secondary roads using a 3-D FE model. The model incorporates measured 3-D tire-pavement contact stresses, HMA linear viscoelasticity, continuous moving loads, and utilizes implicit dynamic analysis. The analyzed pavement structures were comprised of a 76-mm HMA layer and an aggregate base layer with various thicknesses (203, 305, and 457 mm).

Due to having different contact stress distributions at tire-pavement interface, the 455 wide-base tire and the conventional dual-tire assembly impact secondary road pavements in different ways. The wide-base tire causes greater tensile strains and compressive strains but less shear strains in the HMA layer. The pavement responses in the HMA layer are significantly affected by the temperature and unbound base layer thickness. As temperature increases, in addition to the increase of strain magnitudes, more areas of HMA are exposed to the tensile stress state. The maximum tensile strain and compressive strain decrease as the unbound base thickness increases, while the maximum shear strain is not significantly affected by the granular base layer thickness.

Five different failure mechanisms (fatigue cracking, HMA rutting caused by densification and shear, base shear failure, and subgrade rutting) were considered in this analysis of secondary road pavement damage. The 455 wide-base tire causes 1.91-2.50 times more fatigue damage, 1.31-2.35 times more subgrade rutting, and 1.35-1.77 times more HMA rutting (densification) compared to the conventional dual-tire assembly when

carrying the same load. On the other hand, the 455 wide-base tire causes 19%-78% less HMA rutting (shear) and 4%-31% less base shear failure potential than the conventional dual-tire assembly. These damage ratios vary with base layer thicknesses and HMA temperatures. Therefore, the potential damage to secondary roads from using wide-base tires depends on the pavements' predominant failure mechanisms.

A combined damage ratio was used to consider the overall effect of different failure mechanisms on pavement serviceability and to conduct a simplified pavement cost analysis associated with the wide-base tire. In general, the results show that using the 455 wide-base tire results in 1.12-1.38 times more damage compared to the dual-tire assembly and thus greater rehabilitation costs for secondary road pavements. The estimated costs provide state pavement agencies a basis for implementing appropriate load regulations and road pricing for trucking operations. Simple design examples are provided that describe how to consider the effects of wide-base tires in pavement design and rehabilitation practice by using the damage ratio obtained from this study. However, more cases must be evaluated.

Worthy of note is that an earlier study concluded the wide-base tire causes less or similar damage to interstate highway pavements when compared to the dual-tire assembly.

5.2 Recommendations

As a result of this study, the authors make the following recommendations:

1) The traditional static uniform circular loading assumption cannot differentiate between different contact areas and contact stress distributions at the tire-pavement interface. Hence, accurate tire-pavement interaction is essential to evaluate the pavement damage caused by various tire configurations.

2) At this point in time, the mechanistic-empirical method is recommended to quantify pavement damage associated with wide-base tires. The failure mode

for each pavement layer needs to be related to the critical response calculated at a specific position under loading.

3) A large database should be built to consider the effects of wide-base tires in pavement design and rehabilitation practice by using the damage ratio concept. The database needs to consider various pavement structures and axle configurations.

REFERENCES

AASHTO (1993). AASHTO Guide for design of pavement structures. American Association of State Highway and Transportation Officials (AASHTO), Washington D.C.

ABAQUS (2007). ABAQUS/Standard User's Manual Version 6.7, Hibbitt, Karlsson & Sorenson, Inc., Pawtucket, RI.

Al-Qadi, I.L., P.J. Yoo, M.A. Elseifi, and I. Janajreh (2005). Effects of Tire Configurations on Pavement Damage, Journal of the Association of Asphalt Paving Technologists, Vol. 74, p. 921-962.

Al-Qadi, I.L. and M.A. Elseifi (2007). State-of-the-Practice of the New Generation of Wide-Base Tire and its Impact on Trucking Operations, Transportation Research Record, 2008, TRB, Washington, D.C., p. 100-109.

Al-Qadi, I.L., E. Tutumluer, S.H. Dessouky, and J. Kwon (2007). Effectiveness of Geogrid-Reinforcement in Flexible Pavements: A Full-Scale Testing, Final Report to Tensar Earth Technologies, Inc., University of Illinois at Urbana-Champaign.

Al-Qadi I.L., H. Wang, P.J. Yoo, and S.H. Dessouky (2008). Dynamic Analysis and In-situ Validation of Perpetual Pavement Response to Vehicular Loading, Transportation Research Record, 2087, p. 29-39.

Al-Qadi, I.L., and H. Wang (2009a). Full-depth Pavement Responses under Various Tire Configurations: Accelerated Pavement Testing and Finite Element Modeling, accepted by the Journal of the Association of Asphalt Paving Technologists, Vol. 78.

Al-Qadi, I.L., and H. Wang (2009b). Evaluation of Pavement Damage Due to New Tire Designs, Research Report ICT-09-048, Illinois Center for Transportation

ARA, Inc. (2004). ERES Division, Development of the 2002 Guide for the Design of New and Rehabilitated Pavements, NCHRP 1-37A, Transportation Research Board, Washington, D.C.

Asphalt Institute (1982). Research and Development of the Asphalt Institute's Thickness Design Manual (MS-1), Research report 82-1, 9th ed., College Park, MD.

Bathe, K.J. (1982). Finite Element Procedures in Engineering Analysis, Prentice-Hall, NJ.

Bonaquist, R. (1992). An Assessment of The Increased Damage Potential of Widebase Single Tires, Proc. of 7th International Conference on Asphalt Pavements, Vol. 3, International Society for Asphalt Pavements, Lino Lakes, MN, p. 1-16.

Chopra, A.K. (2001). Dynamics of Structures, 2nd ed., Prentice Hall, Upper Saddle River, NJ.

COST 334 (2001). Effects of Wide Single Tires and Dual Tires, Final report of the action, European Cooperation in the Field of Scientific and Technical Research, Brussels, Belgium.

Deacon J.A., J.T. Harvey, I. Guada, L. Popescu, and C.L. Monismith, (2002). Analytically Based Approach to Rutting Prediction, Transportation Research Record, 1806, p. 9-18.

Ferry J.D. (1980). Viscoelastic Properties of Polymers, 3rd ed., Wiley & Sons, New York.

Huang, Y.H. (1993). Pavement Analysis and Design, 1st ed., Prentice Hall, NJ.

Huhtala, M., J. Philajamaki, and M. Pienimaki (1989). Effects of Tires and Tire Pressures on Road Pavements, Transportation Research Record, 1227, TRB, National Research Council, Washington, D.C., p. 107-114.

Illinois Department of Transportation, (2006). Truck Size and Weight Report, Illinois Department of Transportation, Springfield, IL.

Maree, J.H. (1978). Design Parameters for Crushed Stone in Pavements, M. Eng thesis, Department of Civil Engineering, Faculty of Engineering, University of Pretoria, South Africa.

Monismith C. L., R.G. Hicks, F.N. Finn, J. Sousa, J. Harvey, S. Weissman, J. Deacon, J. Coplantz, and G. Paulsen (1994). Permanent Deformation Response of Asphalt Aggregate Mix, SHRP-A-415 Report, Strategic Highway Research Program, National Research Council, Washington, D.C.

Monismith C. L., L. Popescu, and J.T. Harvey (2006). Rut Depth Estimation for Mechanistic-Empirical Pavement Design Using Simple Shear Test Results, Journal of Association of Asphalt Paving Technologists, Vol.75.

Organization for Economic Co-Operation and Development (1992). Dynamic Loading of Pavements, OECD report, OECD, Paris, France.

Priest, A.L., D.H. Timm, and W.E. Barrett (2005). Mechanistic Comparison of Wide-base Single vs. Standard Dual Tire Configurations, Final Report, National Center for Asphalt Technology (NCAT), Auburn, AL.

Theyse, H.L., M. De Beer, and F.C. Rust (1996). Overview of the South African Mechanistic Pavement Design Analysis Method, Transportation Research Record, 1539, p. 6-17.

Theyse, H.L., J.W. Maina, and L. Kannemeyer (2007). Revision of the South African Flexible Pavement Design Method: Mechanistic-Empirical Component, Proc. 9th Conference on asphalt pavements for Southern Africa (CAPSA), Gaborone, Botswana, September 2-5, p. 256-292.

Thompson, M., F. Gomez-Ramirez, E. Gervais, and M. Roginski (2006). Concepts for Developing a Mechanistic-Empirical Based ACN Procedure for New Generation Aircraft, Proc. 10th International Conference on Asphalt Pavement, Quebec, Canada.

Tielking, J.T. and F.L. Roberts (1987). Tire Contact Pressure and Its Effect on Pavement Strain, Journal of Transportation Engineering, vol. 113, no. 1, ASCE, p. 56-71.

Van Gurp, C, and A.J. Van Leest, (2002). Thin Asphalt Pavements on Soft Soil, Proc. 9th International Conference on Asphalt Pavements, International Society for Asphalt Pavements, Copenhagen, Denmark.

Wang, H. and I.L. Al-Qadi (2009). The Combined Effect of Moving Wheel Loading and Three-Dimensional Contact Stresses on Perpetual Pavement Responses, accepted by the Journal of Transportation Research Record, Paper No. 09-1297, Transportation Research Board of the National Academies, Washington, DC, 2009

Yoo, P.J. and I.L. Al-Qadi (2007). Effect of Transient Dynamic Loading on Flexible Pavements, Transportation Research Record, 1990, Transportation Research Board of the National Academies, Washington, DC, p. 129-140.

Yoo, P.J. and I.L. Al-Qadi (2008). Truth and Myth of Fatigue Cracking Potential in Hot-Mix Asphalt: Numerical Analysis and Validation, Journal of Association of Asphalt Paving Technologists, vol. 77, p. 549-590.